NASA CONTRACTOR REPORT

STRUCTURAL MODELING OF AIRCRAFT TIRES

by S. K. Clark, R. N. Dodge, J. I. Lackey, and G. H. Nybakken

Prepared by
THE UNIVERSITY OF MICHIGAN
Ann Arbor, Mich. 48105
for Langley Research Center

NATIONAL AERONAUTICS AND SPACE ADMINISTRATION • WASHINGTON, D. C. • MARCH 1973

1. Report No. NASA CR-2220	2. Government Accession No.	3. Recipient's Catalog No.
4. Title and Subtitle STRUCTURAL MODELING OF AIRCRAFT TIRES		5. Report Date March 1973
		6. Performing Organization Code
7. Author(s) S. K. Clark, R. N. Dodge, J. I. Lackey, and G. H. Nybakken		8. Performing Organization Report No. 05608-16-T (Revised)
		10. Work Unit No. 501-38-12-02
9. Performing Organization Name and Address The University of Michigan Ann Arbor, Michigan 48105		11. Contract or Grant No. NGL-23-005-010
		13. Type of Report and Period Covered Contractor Report
12. Sponsoring Agency Name and Address National Aeronautics and Space Administration Washington, D.C. 20546		14. Sponsoring Agency Code

15. Supplementary Notes

16. Abstract

A theoretical and experimental investigation of the feasibility of determining the mechanical properties of aircraft tires from small-scale model tires was accomplished. The theoretical results indicate that the macroscopic static and dynamic mechanical properties of aircraft tires can be accurately determined from the scale model tires although the microscopic and thermal properties of aircraft tires can not. The experimental investigation was conducted on a scale model of a 40 × 12, 14 ply rated, type VII aircraft tire with a scaling factor of 8.65. The experimental results indicate that the scale model tire exhibited the same static mechanical properties as the prototype tire when compared on a dimensionless basis. The structural modeling concept discussed in this report is believed to be exact for mechanical properties of aircraft tires under static, rolling, and transient conditions.

17. Key Words (Suggested by Author(s)) Aircraft tires Structural modeling Tire mechanical properties	18. Distribution Statement Unclassified - Unlimited	
19. Security Classif. (of this report) Unclassified	20. Security Classif. (of this page) Unclassified	21. No. of Pages 79	22. Price* $3.00

Page Intentionally Left Blank

TABLE OF CONTENTS

LIST OF ILLUSTRATIONS

SYMBOLS

English Letters

C - Couple or moment

c_p - specific heat of tire material

D - tire nominal diameter

E - tire carcass modulus of elasticity in the plane of the shell

F - force on tire

h - heat transfer coefficient between tire and surrounding air

K - thermal conductivity of tire material

k_o - radius of gyration of tire about its axis of rotation

$k_1, k_2, \ldots, k_{10}$ - numerical exponents

k_x, k_y, k_z - tire elastic stiffnesses, or spring rates

L - length

l - contact patch half length

M - mass

p_o - tire inflation pressure

q - pneumatic trail

T - time

V - wheel forward velocity

w - tire section width

Greek Letters

δ - tire deflection

θ - temperature

η - tire damping coefficient

λ - tire relaxation length

μ - Poisson's ratio of tire materials

Π - dimensionless factors

ρ - tire material density

σ - tire stress

ψ - yaw angle or angle of rotation of tire about a vertical, or steer, axis

Subscripts

m - model

p - prototype

x,y,z - co-ordinate directions according to Figure 2

ψ - direction normal to wheel plane

E - energy

F - force

STRUCTURAL MODELING OF AIRCRAFT TIRES

By

S. K. Clark, R. N. Dodge, J. I. Lackey, and G. H. Nybakken

SUMMARY

Techniques have been developed for producing small scale models of aircraft tires. It has been shown that such a scaling can be achieved in theory for the mechanical properties of aircraft tires, both static and dynamic, as well as for the overall or macroscopic stress state of such tires but not for their detailed or microscopic stress state. The question of thermal modeling is still unresolved but theoretical indications are that tire temperature distributions will not be similar or analogous between model and prototype.

Experiments have been conducted on a small scale model of a 40 x 12, 14 PR, Type VII aircraft tire, with a scaling factor of 8.65. Agreement is excellent between the basic static tire mechanical characteristics in model and prototype, referred to a dimensionless basis.

The structural modeling concept discussed in this report is believed to be exact for mechanical properties of an aircraft tire, including static, rolling and transient conditions.

INTRODUCTION

Measurement of the mechanical properties of aircraft tires is an expensive
and lengthy process. Such tires normally tend to be rather heavily loaded
as compared with conventional automobile and truck tires, and to be run at quite
high speeds, so that equipment to simulate field operating conditions is large
and expensive. Only one major facility exists in the United States for the con-
trolled study of aircraft tire characteristics under landing conditions. This
is the well known Landing Loads Simulator track at NASA, Langley Field, Virginia.

Considerable interest exists in obtaining dynamic or transient properties
of aircraft tires for use in shimmy analysis work. A number of recent attempts
at shimmy analysis followed by actual landing gear experience lead one to be-
lieve that current shimmy theories, using static mechanical properties of air-
craft tires, are not now capable of clearly defining the shimmy characteristics
of an aircraft landing gear system. There seems to be no obvious flaw in the
theoretical formulation of shimmy calculations. One possible short-coming lies
in the use of the elastic properties of tires as determined by static tests.
If such properties could be determined under dynamic conditions, the values
might be different enough so that better agreement between shimmy theory and
experience would ensue. Such data is difficult to obtain on full size tires,
again due to the size and complexity of the equipment needed to produce the ap-
propriate operating conditions for the tires.

In addition, problems occur from time to time in aircraft tire operation
which can only be solved by tests involving specific conditions. Such tests

2

may be difficult and expensive due to limited facilities, or due to the size and complexity of the equipment needed at these facilities, or due to safety considerations.

It was felt desirable to review the possibility of structural modeling of aircraft tires, with the general thought that if such models could be developed then they could be used to predict the effect of dynamic factors upon static mechanical tire data by reproducing the actual operating conditions of the aircraft tire. Such simulation, done on a small scale, should be much easier and more economical to carry out than actual full scale measurements. In addition, there would be available a scale modeling tool which could be useful in supplementing full scale tests, and in some limited cases even replacing such tests. It would appear that the ability to produce a scale model aircraft tire which is capable of quantitative interpretation would be a valuable contribution to aircraft preliminary design, as well as to many practical operating problems.

THEORY OF MODELING

The theory of tire modeling may be divided into three separate categories or sets of modeling requirements, involving tire mechanical properties, tire stresses and tire temperatures. These will be discussed separately.

MODELING OF TIRE MECHANICAL PROPERTIES

The first, and least restrictive, case is modeling of tire mechanical properties, which is the primary concern of this report. For that purpose, consider the tire mechanical properties, both static and dynamic, to be defined by the following engineering variables, as illustrated in Figure 1.
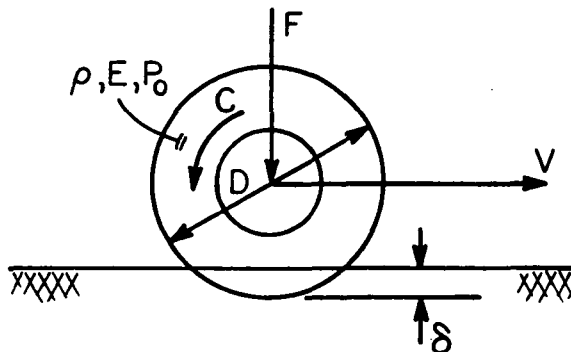
Figure 1. Tire geometry and nomenclature.

where F = load on the tire

C = moment on the tire

D = tire diameter, a characteristic length*

E = Young's modulus for the tire material

μ = Poisson's ratio for the tire material

---

*Any characteristic length is satisfactory, but tire diameter is a readily available measure of size.

4

p_o = tire inflation pressure

δ = tire deflection

ρ = tire material density

k_o = radius of gyration of tire and wheel

It should be noted that the tire carcass properties are represented as single quantities E and μ, although in actuality they are distributions of elastic properties throughout the carcass. This dimensionless distribution must be maintained in the model tire exactly as in the full size tire in order for modeling to be exact. This is a requirement which is analogous to the need for geometric similarity between model and prototype, a well known and universally accepted condition.

Several obvious dimensionless variables may be identified by inspection. These are

Π_1 = complete geometric similarity between model and prototype, including the dimensionless distribution of elastic properties between model and prototype for the tire carcass.

Π_2 = δ/D

Π_3 = $\dfrac{k_o}{D}$

Π_4 = $\dfrac{p_o}{E}$

Π_5 = μ

Π_6 = $\dfrac{FD}{C}$

The remaining terms may be written in a general functional relation using a typical dependent property, the relaxation length λ of the tire. One may express this as a function of the pertinent engineering variables remaining as

$$\left(\frac{\lambda}{D}\right) = f(F, V, p_o, D, \rho) \tag{1}$$

The method used to obtain the dimensionless variables from a relationship such as Eq. (1) will be taken from Langhaar [1], and will not be derived here. Using Langhaar's notation, the dimensional matrix for the pertinent engineering variables is given by Eq. (2):

$$
\begin{array}{c|ccccc}
 & F & V & p_o & D & \rho \\
\hline
M & 1 & 0 & 1 & 0 & 1 \\
L & 1 & 1 & -1 & 1 & -3 \\
T & -2 & -1 & -2 & 0 & 0 \\
\end{array}
\tag{2}
$$

Let the functional relationship between the relaxation length and the other variables be of the form

$$\left(\frac{\lambda}{D}\right) = f\left(F^{k_1} V^{k_2} p_o^{k_3} D^{k_4} \rho^{k_5}\right) \tag{3}$$

Then the exponents are related through the expressions

$$k_1 + k_3 + k_5 = 0$$

$$k_1 + k_2 - k_3 + k_4 - 3k_5 = 0 \tag{4}$$

$$-2k_1 - k_2 - 2k_3 = 0$$

6

In Eq. (4), the unknown exponents k_3, k_4, k_5 may be expressed in terms of k_1 and k_2 in the form

$$k_5 = -k_1 - k_3 = -k_1 + k_1 + \frac{1}{2} k_2 = \frac{1}{2} k_2$$

$$k_4 = -2k_1 \tag{5}$$

$$k_3 = -k_1 - \frac{1}{2} k_2$$

The dimensionless terms governing the relaxation length may now be expressed as a dimensionless matrix of coefficients:

$$
\begin{array}{c|ccccc}
 & k_1 & k_2 & k_3 & k_4 & k_5 \\
\hline
\Pi_7 & 1 & 0 & -1 & -2 & 0 \\
\Pi_8 & 0 & 1 & -1/2 & 0 & 1/2
\end{array}
\tag{6}
$$

From this, one obtains two additional Π terms which must be held constant in order that the model and prototype are identical:

$$\Pi_7 = \left(\frac{F}{p_o D^2}\right) \qquad \Pi_8 = \left(\frac{v^2 \rho}{p_o}\right) \tag{7}$$

$$= \left(\frac{v^2 \rho}{E}\right) \quad \text{using } \Pi_4$$

Of these terms, Π_8 is the ratio of tire velocity to a characteristic wave velocity, and is similar in concept to a Mach number. Π_7 is, however, the important scaling parameter since it relates the tire inflation pressure p_o, tire diameter D and the force acting on the tire between model and prototype. In view of the fact that complete geometric similarity is an additional requirement,

then any appropriate tire section width, tire diameter, or tire section height could be used in place of the diameter D in Π_7 so long as the dimensional character of that term remains the same. The Russian R. K. Gordon [2] has arrived at Π_7 by a somewhat different line of reasoning.

A short discussion of the scaling parameter Π_7 is in order. If the inflation pressures for model and prototype are known, and if the relative sizes of model and prototype are known, then the appropriate forces between model and prototype may be determined by the fact that Π_7 must be equal for model and prototype in a given test situation. The scale ratio or model diameter D is at the choice of the experimenter. The pressure p_o must, however, be determined in conjunction with the required equality for Π_4. This latter term demands that the ratio of inflation pressure of the model tire to its modulus of elasticity must be identical to that ratio in the full size prototype. Under those conditions, it may be seen that one may construct the small size model of a large aircraft tire using a purposely lower modulus of elasticity in the small model. This will allow a lower inflation pressure p_o, since in the model the ratio (p_o/E) must remain the same as in the prototype. This further means that in evaluating the dimensionless term Π_8, the influence of velocity of travel will be amplified in the model. For example, if in the model it is possible to use a low modulus of elasticity and a relatively low pressure, reference to Eq. (7) shows that the model velocity can be made significantly higher. This is seen by equating Π_8 for the model and prototype, and solving for the model velocity. This gives

$$V_m = \sqrt{\left(\frac{E_m}{E_p}\right)\left(\frac{\rho_p}{\rho_m}\right)}\ V_p \qquad (8)$$

8

where the subscripts m and p refer to model and prototype, respectively.

If the material densities of the prototype and model are essentially the same, Eq. (8) shows that the model velocity V_m needed to obtain an equivalent prototype velocity V_p may be substantially less than the prototype velocity by the ratio of the square root of the model tire modulus to the prototype modulus. Methods of controlling tire modulus are available and may be used to advantage here. In effect, high speed tire testing on the model can be conducted at relatively low speeds.

In general, this dimensional analysis shows that a typical tire response quantity, relaxation length λ, is related to the dimensionless Π terms through the relationship

$$\frac{\lambda}{D} = f(\Pi_1, \Pi_2, - - - - - \Pi_8) \tag{9}$$

If the dimensionless relaxation length λ/D is to be the same in both model and prototype, then each of the terms Π_1 through Π_8 must be the same in model and prototype. As discussed, this can be achieved by the use of geometric similarity, by the use of the same materials, but with the degree of freedom that the model tire elastic modulus may be substantially reduced over that of the prototype provided that the modulus distribution is analogous or geometrically similar in both cases. This will allow all Π terms to remain the same and will allow enhancement of velocity effects, which is desirable for high speed tire testing. In effect, $\Pi_4 = p_o/E$ represents the primary independent variable of this analysis, since the modulus of elasticity of the tire carcass materials represents one distinct input decision. The second basic variable is $\Pi_2 = \delta/D$,

9

which defines a length scaling. From this, it may be concluded that tire

mechanical properties may be readily modeled between full size tire and small

scale tire provided that one learns how to use tire materials in such a way

that the distribution of carcass stiffness or elastic constants is the same

between model and prototype, and that preferably the absolute level of the

elastic constants be significantly reduced in the model compared to the proto-

type, without changing the relative or dimensionless distribution.

MODELING OF TIRE STRESS LEVELS

A second level of sophistication in tire modeling theory may be brought

about by attempting to model the internal stress state between small scale

model and prototype, in addition to the appropriate mechanical properties.

Let us in this case imagine that the tire stress state is governed by the same

engineering variables as shown in Figure 1, where all symbols are the same as

before except for the stress level σ.

It is recognized from the previous dimensional analysis that six dimension-

less products must be automatically satisfied by any model. These are

Π_1 = complete geometric similarity, including distribution

   of elastic constants (10)

$$\Pi_2 = \frac{\delta}{D} \tag{11}$$

$$\Pi_3 = k_o/D \tag{12}$$

$$\Pi_4 = \frac{p_o}{E} \tag{13}$$

10

$$\Pi_5 = \mu(\text{Poisson's ratio}) \tag{14}$$

$$\Pi_6 = FD/C \tag{15}$$

Assuming these to be true, the stress state in the moving tire may now be expressed in the general functional form

$$\frac{\sigma}{p_o} = f(p_o, D, V, F, \rho) \tag{16}$$

The right-hand side of Eq. (16) is identical to that of Eq. (1), so that the dimensionless quantities governing this are identical to those previously gotten in Eq. (7), i.e.,

$$\Pi_7 = \frac{F}{p_o D^2} \tag{17}$$

$$\Pi_8 = \frac{V^2 \rho}{E} \tag{18}$$

Now one may write

$$\sigma = p_o f(\Pi_1, \Pi_2, - - - - -\Pi_8) \tag{19}$$

Equation (19) shows that if one wishes to maintain the same stress level in model and prototype, then all terms $\Pi_1, - - - - - \Pi_8$ must be held identical, and in addition the inflation pressure p_o must be the same in both model and full size tire. Since p_o must be constant, then from Π_4 (Eq. (13)) it is seen that modulus of elasticity E of both model and full size tire must also be the same. In effect, this forces one to use the same materials for the model as the full size tire.

11

The rules for one form of modeling a full size tire to small scale can now be seen by a study of Eqs. (10) through (19). For example, the requirement of complete geometric similarity again means that the small scale tire should be geometrically proportional in all respects to the original tire. Since it is necessary to use the same inflation pressure in the small scale tire as in the full size tire, Eq. (13) requires that the modulus of elasticity E remain the same in the model as in the prototype. Then the stress level expressed in Eq. (19) will remain the same between the small scale and full size tire. Equation (11) shows that the dimensionless deflection of the tire should be the same on the model as on the full size tire. Equation (14) shows that the Poisson's ratio of the material used to make the model tire should be the same as that of the full sized tire, and this will of course be automatically satisfied if the same materials are used. In addition, the distribution of cord angles and materials should be identical between model and prototype. Equation (17) shows that under these conditions, the load applied to the model tire should be in the ratio of the square of the scale factor. For example, if the model tire is one fifth of the size of the full tire, then a load equal to one twenty-fifth of the full scale load should be applied to the model tire. Finally, Eq. (18) shows that the model tire should be run at the same surface speed as the full size tire, since both the material density ρ and the Young's modulus E of the material will be the same in both model and full size tire.

If all of these conditions are met, then Eq. (19) predicts that the over-all or macroscopic stress state in the model tire will be the same as in the full size tire.

It should be noted that this set of requirements is somewhat stricter and more confining than the previous set which dealt with mechanical properties of the tire alone. Here, the pressure is specified as is the modulus of elasticity of the model tire material. This was not the case in the previous analysis describing only mechanical properties, where it was possible to reduce modulus and pressure simultaneously and still retain dimensional similarity. This simply means that in the previous case, the stress levels in the model tire were not equal to those in the prototype. Here, where equal stress levels are desired, the additional restrictions of pressure and modulus equality are necessary.

In order that this situation be understood more clearly, it should be mentioned that in a practical sense it is essentially impossible to insure that a textile-cord structure be made in small scale that is identical in all respects to a similar structure in large size. Textile cords are manufactured only in discrete sizes and in general cannot be scaled downward arbitrarily. The details of aircraft tire construction are sometimes so numerous as to render the construction of a completely similar small model almost impossible, even though the overall, macroscopic constants of the tire carcass material may be successfully modeled. For these reasons it is very probable that such effects as durability and failure will be very difficult to assess on a scale model with any significant scale ratio simply due to the basic unavailability of the proper materials, and the great difficulty of producing a completely geometrically similar structure. Put in other terms, the detailed construction cannot be modeled practically, so that the microscopic or local stress state will not be equal between model and prototype.

13

In the event that such tire stress comparisons are desired, it should again be emphasized that the modulus of elasticity, or elastic constants, of the model and full size tire must be held the same, that the inflation pressure of the model must be identical to that of the prototype, and that the surface speeds must also be equal between the two. Under these conditions, forces proportional to the square of the scale factor arise between model and prototype, as indicated by Eq. (17), while the overall or macroscopic internal stress state of the model tire is the same as the full size tire.

MODELING OF TIRE EQUILIBRIUM TEMPERATURE

Now consider the somewhat more complex case of including in the analysis the quantities which determine the equilibrium temperature of the running tire. In order to do this, we adopt Eq. (20) as a basic statement of functional dependence.

$$\frac{K\theta}{\rho V^3 D} = f(p_o,\ D,\ V,\ F,\ \rho,\ c_p,\ K,\ h) \tag{20}$$

where the new symbols are as follows:

K = thermal conductivity of tire material

θ = temperature

c_p = specific heat of tire material

h = heat transfer coefficient between tire and atmosphere.

The particular form of the left-hand side of Eq. (20) is chosen so as to represent temperature in a dimensionless fashion. Other representations are possible, but do not lead to anything different. The dimensional matrix involving these

14

variables is shown in the table below, where temperature θ is taken as a basic physical variable.

	F	V	p_o	D	ρ	c_p	K	h
M	1	0	1	0	1	0	1	1
L	1	1	-1	1	-3	2	1	0
T	-2	-1	-2	0	0	-2	-3	-3
θ	0	0	0	0	0	-1	-1	-1

$$\text{(21)}$$

A dimensional analysis of these variables leads to the following dimensionless characteristics which must be equal between model and prototype, over and above those given by Eqs. (10) through (19), previously derived:

$$\Pi_7 = \frac{K}{Dh} \tag{22}$$

$$\Pi_8 = \frac{h}{V \cdot \rho \cdot c_p} \tag{23}$$

Of these two dimensionless quantities, Eq. (23) will be automatically satisfied provided that the conditions described in the previous dimensionless analysis are fulfilled, that is, the velocity of running and density of the tire material are the same between model and prototype. The heat transfer coefficient h and the material specific heat c_p will be approximately the same in the full size tire as in the model, so that Eq. (23) will be automatically the same for both model and prototype.

However, Π_7 very probably will not be equal between model and prototype, since the heat transfer coefficient h and thermal conductivity K of both model and full size tires will be approximately the same, while the characteristic

15

length D will vary as the scale factor. Based on this, Eq. (20) may be rewritten as

$$\theta = \frac{v^2}{c_p} f(\Pi_1, \Pi_2, \Pi_3, \Pi_4, \Pi_5, \Pi_6, \Pi_7, \Pi_8) \qquad (24)$$

From this, it may be seen that the temperature θ of the model tire will be the same as that of the prototype provided that the velocity of travel and the specific heat of the tire material are the same as in the full size tire, and in addition that all of the dimensionless factors Π_1 through Π_8 are held constant between the scale model and the full size tire. As was just discussed, it is possible to do this with the exception of the single dimensionless factor Π_7. Its influence on the equilibrium temperature is not known but may be substantial, since in effect it represents the ratio between the volume of the tire which generates heat due to hysteresis loss, and the convective heat transfer surface area of the tire. It is possible under particularly fortuitous conditions that a good approximation of the full size equilibrium temperature may be obtained from a model tire, but it appears that no guarantee of this exists. Therefore, it is concluded that in general thermal modeling of aircraft tire temperature rise may not be possible without extensive experimentation and the development of suitable scaling factors based on experimental data.

STATIC LOAD-DEFLECTION PROPERTIES OF MODEL AND PROTOTYPE TIRES.

From the discussion in the previous section, it is seen that the structural

modeling of an aircraft tire can only be assured if the pertinent dimensionless

variables are the same for both model and prototype. In general this means that

such quantities must be measured for both tires and compared. In this work, the

method used to do this relies on the measurement of several force-deflection and

geometric relationships in the model, followed by comparison with known full-size

tire data for these same properties.

In accordance with the previous section, all models are geometrically simi-

lar dimensionally and are approximately scaled in their cord content, although

the individual cord size has not been so scaled.

To facilitate an understanding of the various loading situations used in

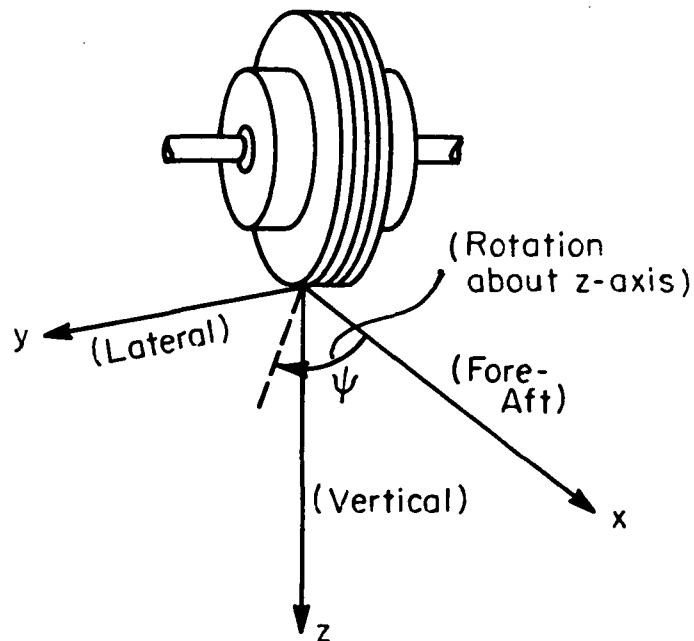this report, a co-ordinate system as shown in Figure 2 has been chosen.

Figure 2. Tire co-ordinate directions.

17

With this co-ordinate system, then, fore-aft, lateral, and vertical forces applied to the tire's contact patch have been denoted by F_x, F_y, and F_z, respectively. A similar notation is used for the appropriate deflections, δ_x, δ_y, and δ_z. A couple or twisting moment about the z-axis has been termed C_z, and the resultant angle of rotation, ψ.

It is possible to use Π_7, Π_6, and Π_2 to describe basic load-deflection relations in a dimensionless way so as to compare the prototype tire with the model tire. Four basic mechanical properties have been chosen since they can be easily measured:

(1) Vertical Load-Vertical Deflection -- (F_z vs. δ_z)

(2) Lateral Load-Lateral Deflection -- (F_y vs. δ_y)

(3) Fore-Aft Load-Fore-Aft Deflection -- (F_x vs. δ_x)

(4) Twisting Moment-Rotation -- (C_z vs. ψ).

Each of these quantities may be expressed in a dimensionless way using the dimensionless variables Π_2, Π_6, and Π_7:

(1) Vertical Load-Vertical Deflection -- $\left(\dfrac{F_z}{p_o D^2} \text{ vs. } \dfrac{\delta_z}{D} \right)$

(2) Lateral Load-Lateral Deflection -- $\left(\dfrac{F_y}{p_o D^2} \text{ vs. } \dfrac{\delta_y}{D} \right)$

(3) Fore-Aft Load-Fore-Aft Deflection -- $\left(\dfrac{F_x}{p_o D^2} \text{ vs. } \dfrac{\delta_x}{D} \right)$

(4) Twisting Moment-Rotation -- $\left(\dfrac{C_z}{p_o D^3} \text{ vs. } \psi \right)$.

Using these dimensionless parameters, comparisons with the prototype can be made to gauge how well the model tire matches it.

These four load-deflection relations are extremely important since they span a wide range of tire deformation effects, from that of an inflated membrane to that of an elastic sheet. Some previous analytical and experimental studies by the authors [3], [4], [5] lead us to believe that most tire mechanical properties may be viewed as the sum or interaction of contributions from the inflated nature of the tire, acting as a gas envelope, and from the elastic nature of its carcass. If the four load-deflection relations just listed are the same, on a dimensionless basis, between model and prototype, then it is strong evidence that all tire mechanical properties are adequately modeled. This is because:

(1) Vertical load-deflection appears to be primarily an inflation pressure effect for aircraft tires. See Ref. [3].

(2) Lateral load-deflection, twisting moment-rotation, and fore-aft load-deflection appear to be a mixture of both inflation and carcass elasticity effects. See Refs. [4] and [5].

Because tire structural differences, mostly cord angle differences, influenced fore-aft load-deflection data, all the model tires were normalized to one fore-aft load-deflection curve. Using Π_2 and Π_7

$$(p_o)_m = \frac{(k_x)_m}{(k_x)_p} \cdot \frac{(D)_p}{(D)_m} \cdot (p_o)_p \tag{25}$$

Then using this $(p_o)_m$ and Π_7 again, we have

$$(F_z)_m = \frac{(p_o D^2)_m}{(p_o D^2)_p} \cdot (F_z)_p \tag{26}$$

19

These two equations outline a procedure to find rated inflation and vertical load for all other tests.

The heuristic estimate of 6800 lb/in. for $(k_x)_p$ was used in Eq. (25) to find the rated inflation pressure. Then Eq. (26) was used to find rated load. These conditions for the four model test tires are given in Table I. This procedure insures that the fore-aft load-deflection data for the four model tires will coincide with the estimated reference stiffness. It then remains to check other mechanical properties to see if one has attained a successful modeling of the prototype.

TABLE I

TIRE OPERATING CONDITIONS

Tire	p_o (psi)	F_z (lb)	D (in.)	w* (in.)
40 x 12 - 14 PR Type VII Prototype	95	14500	39.3	12.12
Model A-18 (2 Ply, 840/2 Nylon, 10 EPI)	25	48.2	4.57	1.67
Model A-15 (2 Ply, 840/2 Nylon, 10 EPI)	23	48.2	4.58	1.66
Model A-14 (2 Ply, 840/2 Nylon, 10 EPI)	19	38.2	4.58	1.64
Model A-13 (2 Ply, 840/2 Nylon, 10 EPI)	20	38.2	4.56	1.62

*w = Section Width

It is worth noting at this point that all data given for the model tires in this report are for exercised tires. It was discovered very early in the

project that the mechanical properties of the model tires became stable only after they had been exercised for a period of time on a road wheel. These changes were most pronounced at low inflation pressures, as one would expect. Consequently, every tire was "run in" for three or four hours at fairly moderate conditions, being the scaled equivalent of about 60 mph speed, 6000 lb vertical load, and 60 psi inflation pressure.

Static load-deflection properties of several model tires, specially constructed to scale the 40 x 12 14 PR prototype (see Appendix), are shown in Figures 3 through 6. Table I lists the operating conditions for each of the models as well as for the prototype. The vertical load F_z shown in the table was that used when obtaining twist, fore-aft, and lateral data.
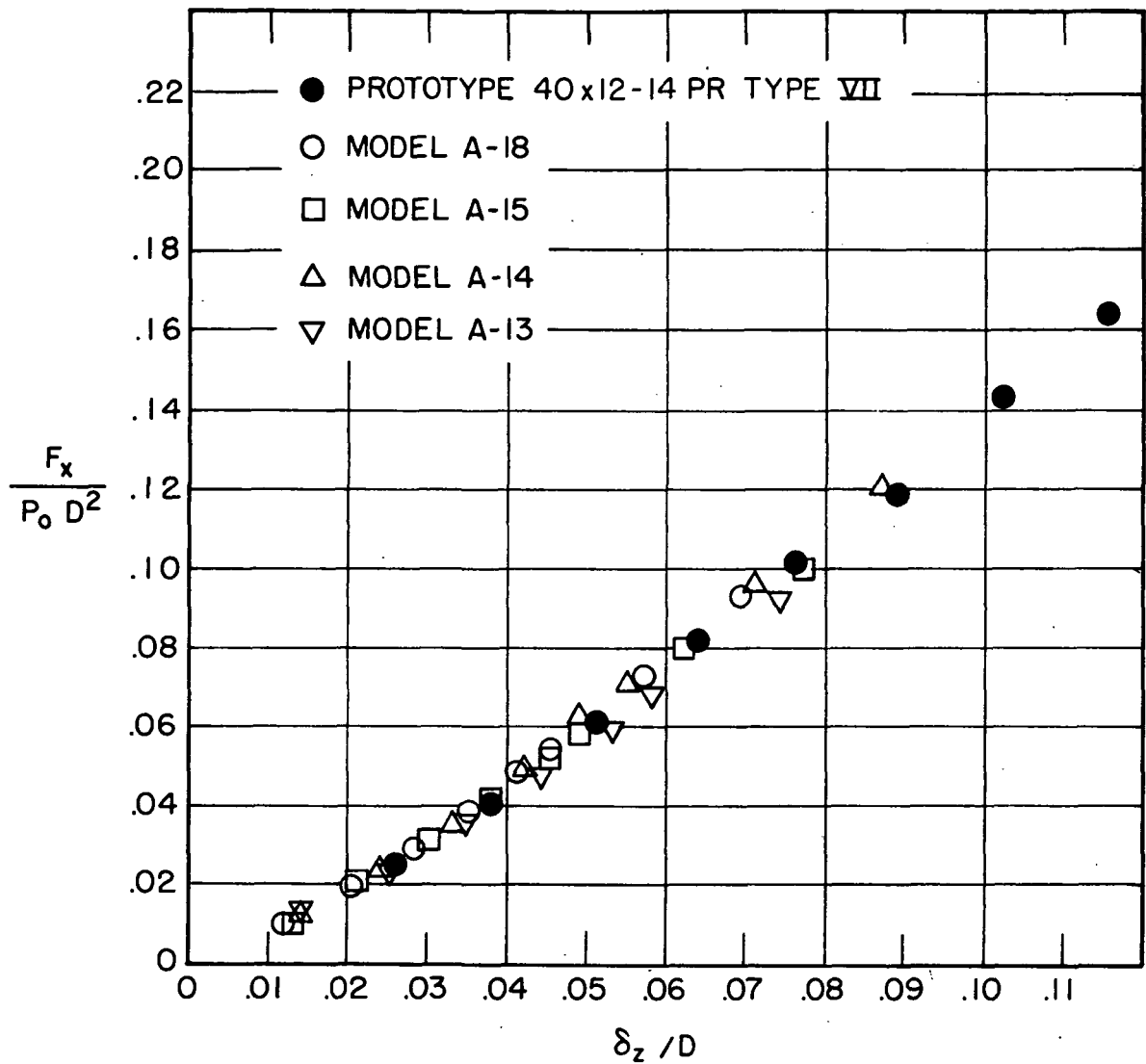
Figure 3. Vertical load-vertical deflection data for model and prototype tires.
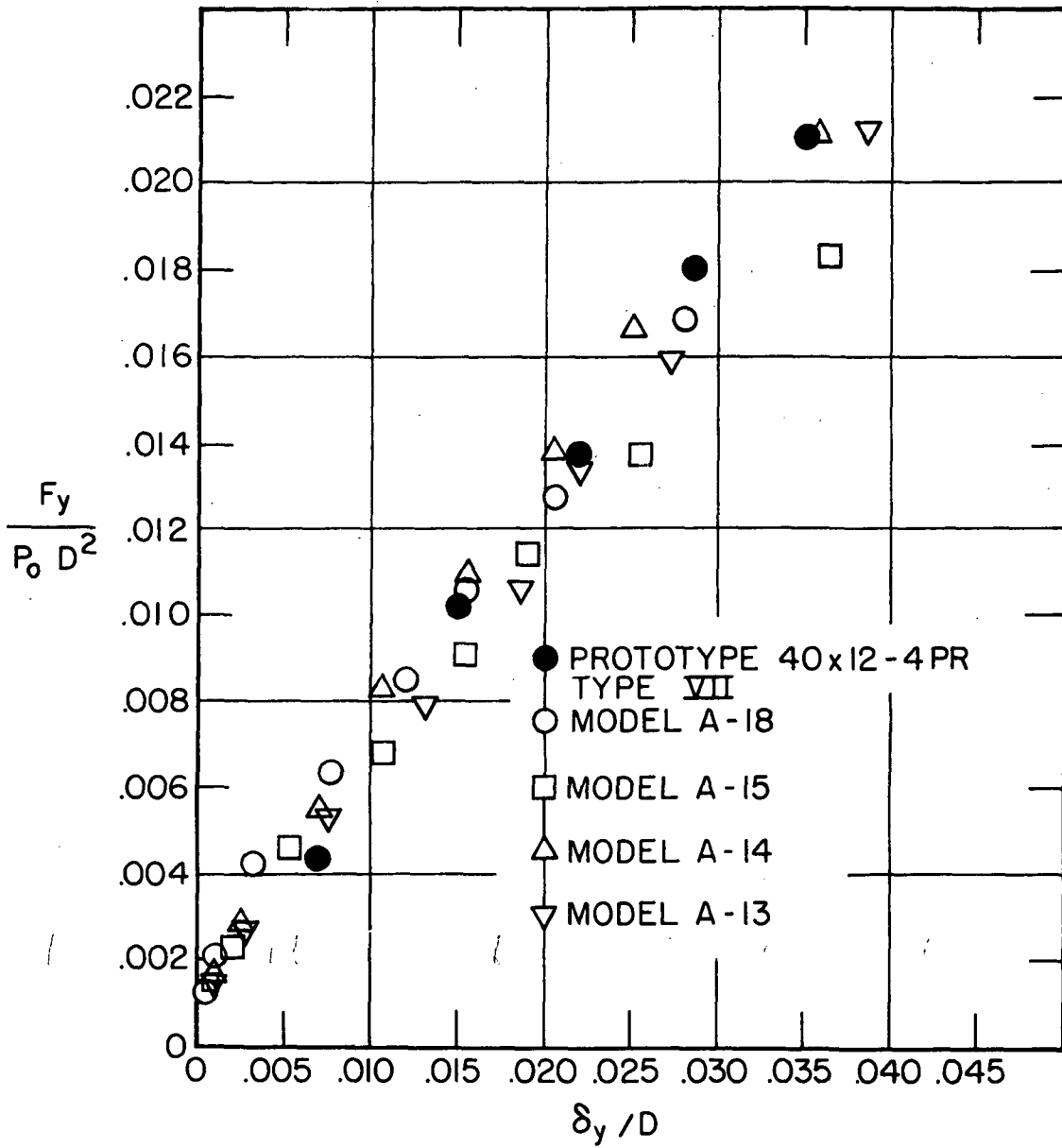
Figure 4. Lateral load-lateral deflection data for model and prototype tires.
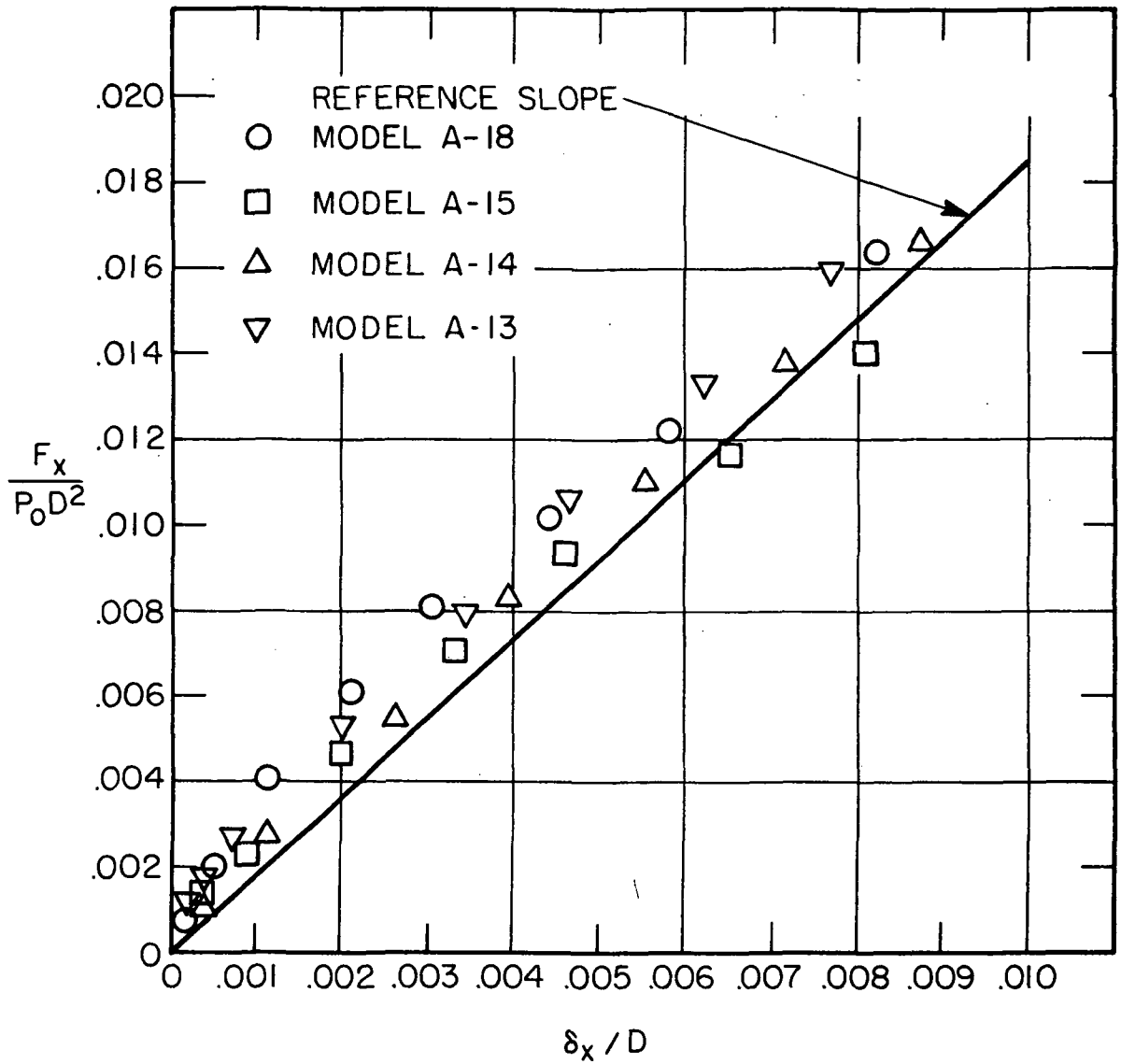
Figure 5. Fore-aft load-deflection data for model tires.
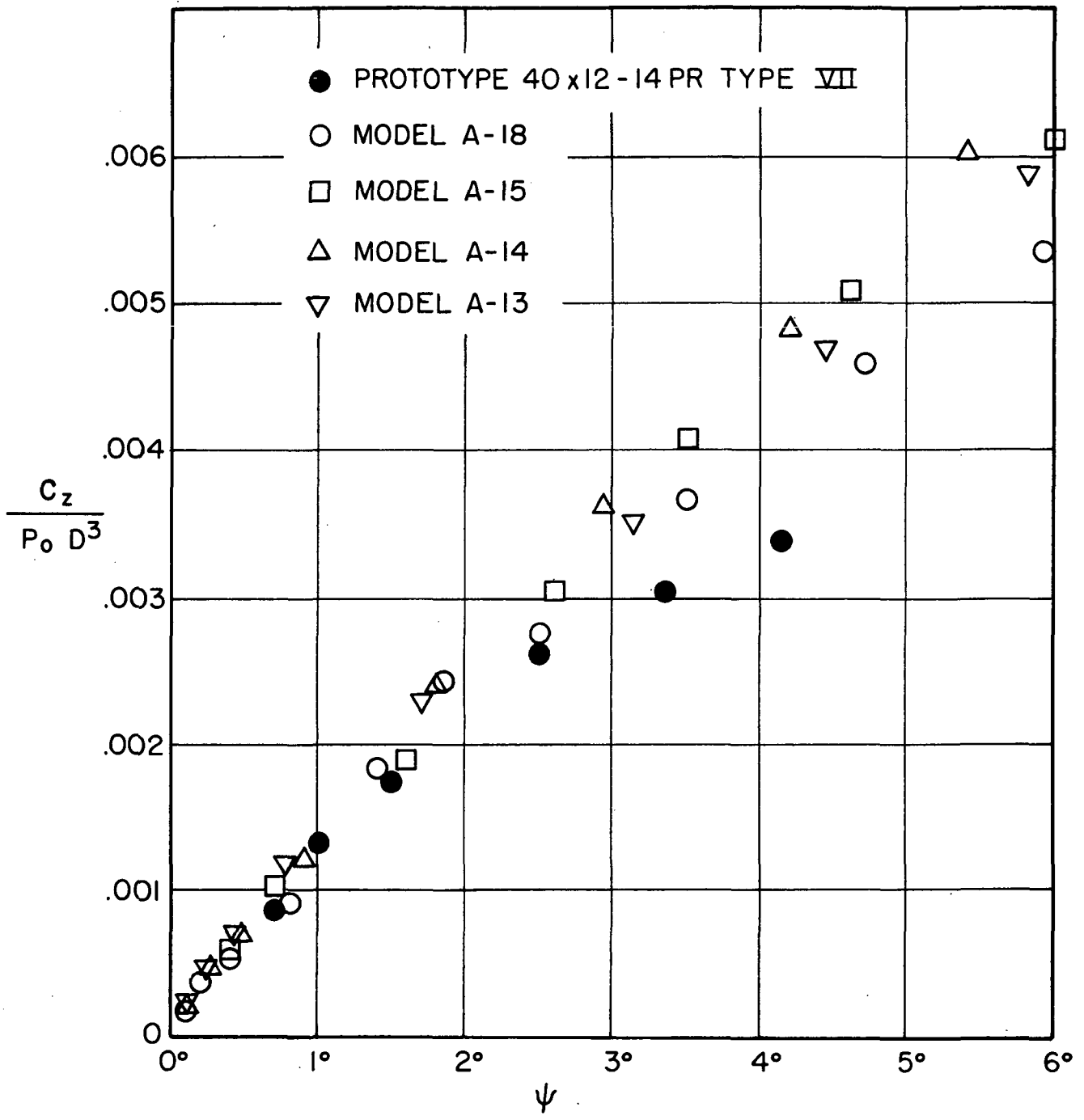
Figure 6.   Twisting moment-rotation data for model and prototype tires.

GEOMETRIC AND SLOW-ROLLING PROPERTIES OF MODEL AND PROTOTYPE TIRES

A previous section has shown that elastic modeling of an aircraft tire can only be assured if certain dimensionless quantities are the same in both model and prototype. In order to assure a comparable basis for comparison of data, the following dimensionless variables are used in discussing the mechanical properties measured in this section:

(a) The tire contact patch half length is expressed by the dimensionless ratio ℓ/D, where D is the tire characteristic length, in this case the outside tire diameter.

(b) Lateral damping coefficient η_y is by definition dimensionless.

(c) Yawed-rolling relaxation length λ_y/D.

(d) Self-aligning torque $(C_z/p_o D^3)$.

(e) Side force $(F_\psi/p_o D^2)$.

(f) Pneumatic trail (q/D).

Summaries of the comparisons of the six tire mechanical properties, measured on four different model tires, with the full size data taken from 40 x 12 tire are shown in Figures 7 through 12. The model tires used for these measurements were previously used in determining the static load-deflection properties in the previous section.

The tire contact patch half length is shown for the model and full size tires in Figure 7. This is a static tire property and generally the model tires tested show contact patch lengths which agree well with the full size tire, the variation between model tires probably being due to minor structural variations.
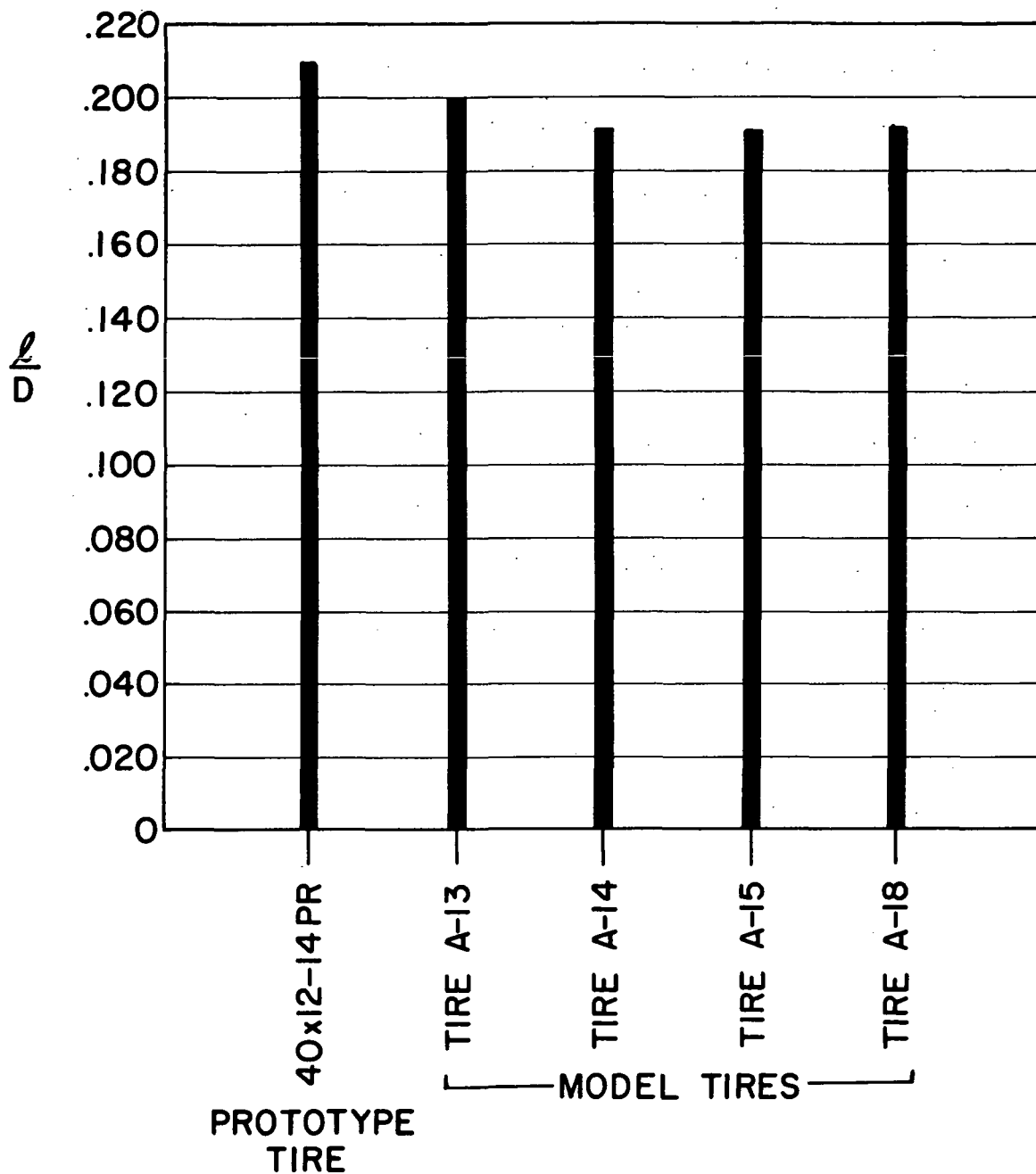
26

Figure 7. Tire half contact-patch length
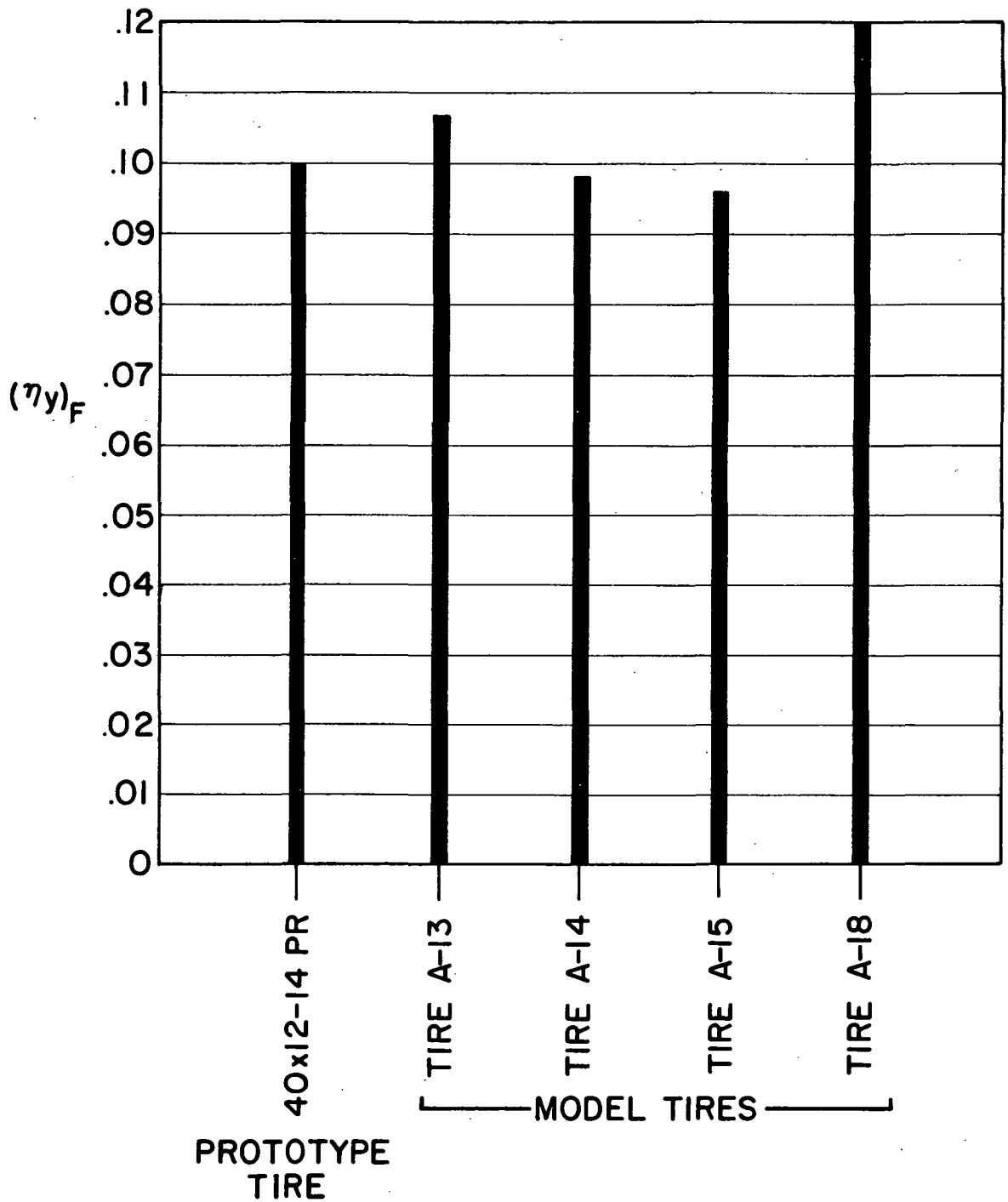data for model and prototype tires.

Figure 8. Lateral damping coefficient data for model
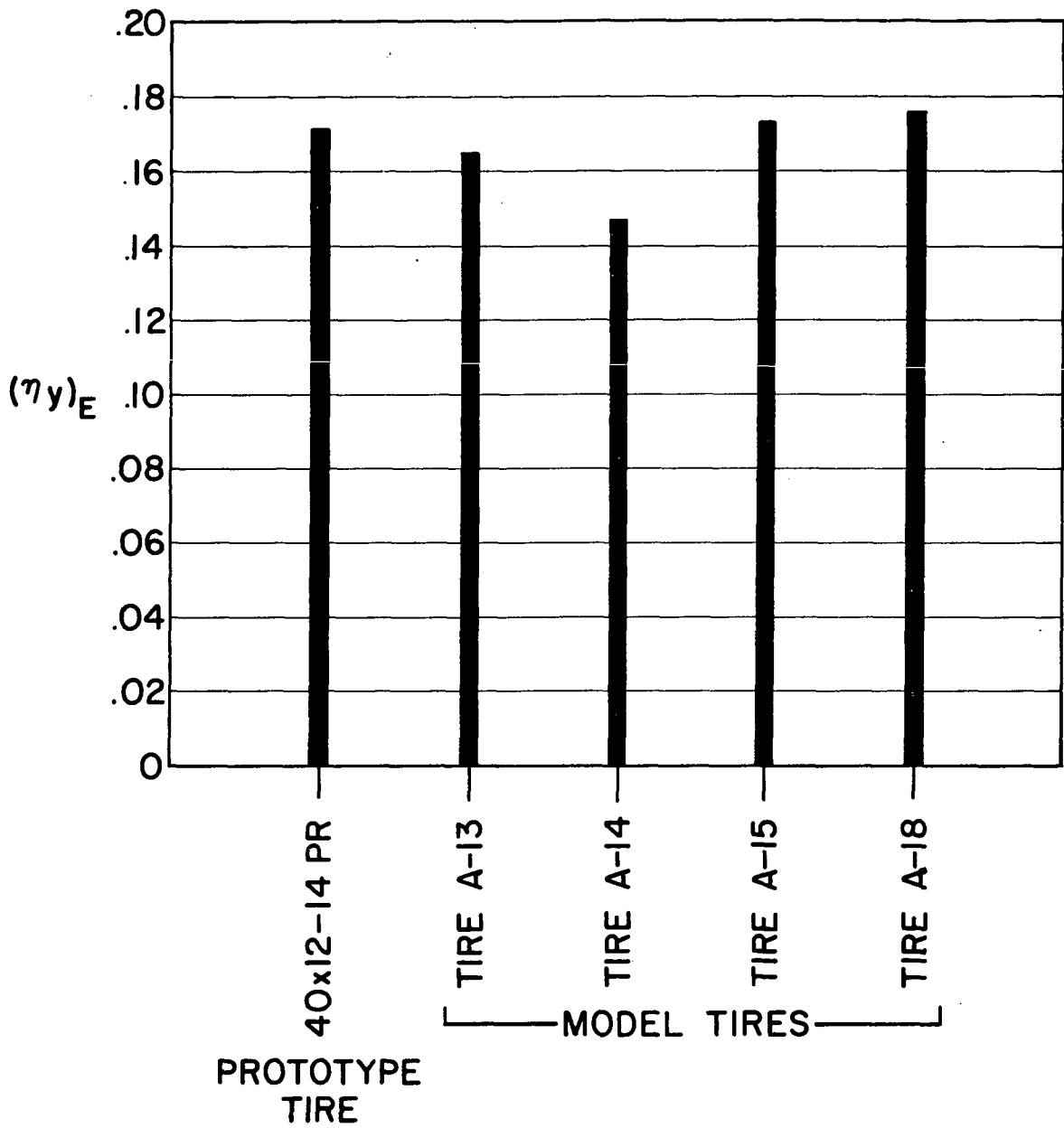and prototype tires, $(\eta_y)_F$ based on force ratio.

Figure 9. Lateral damping coefficient data for model and prototype tires, $(\eta_y)_E$ based on energy ratio.
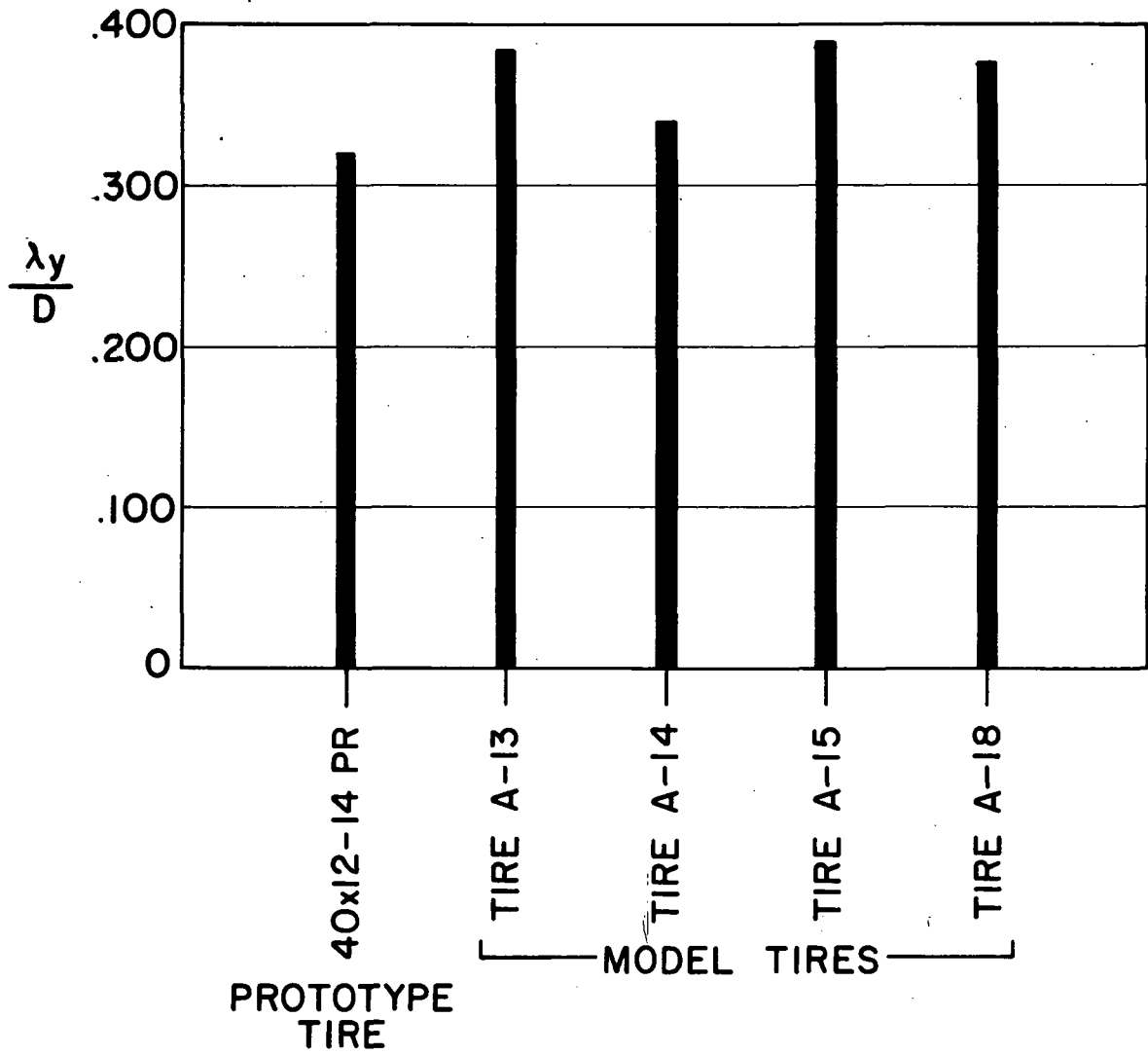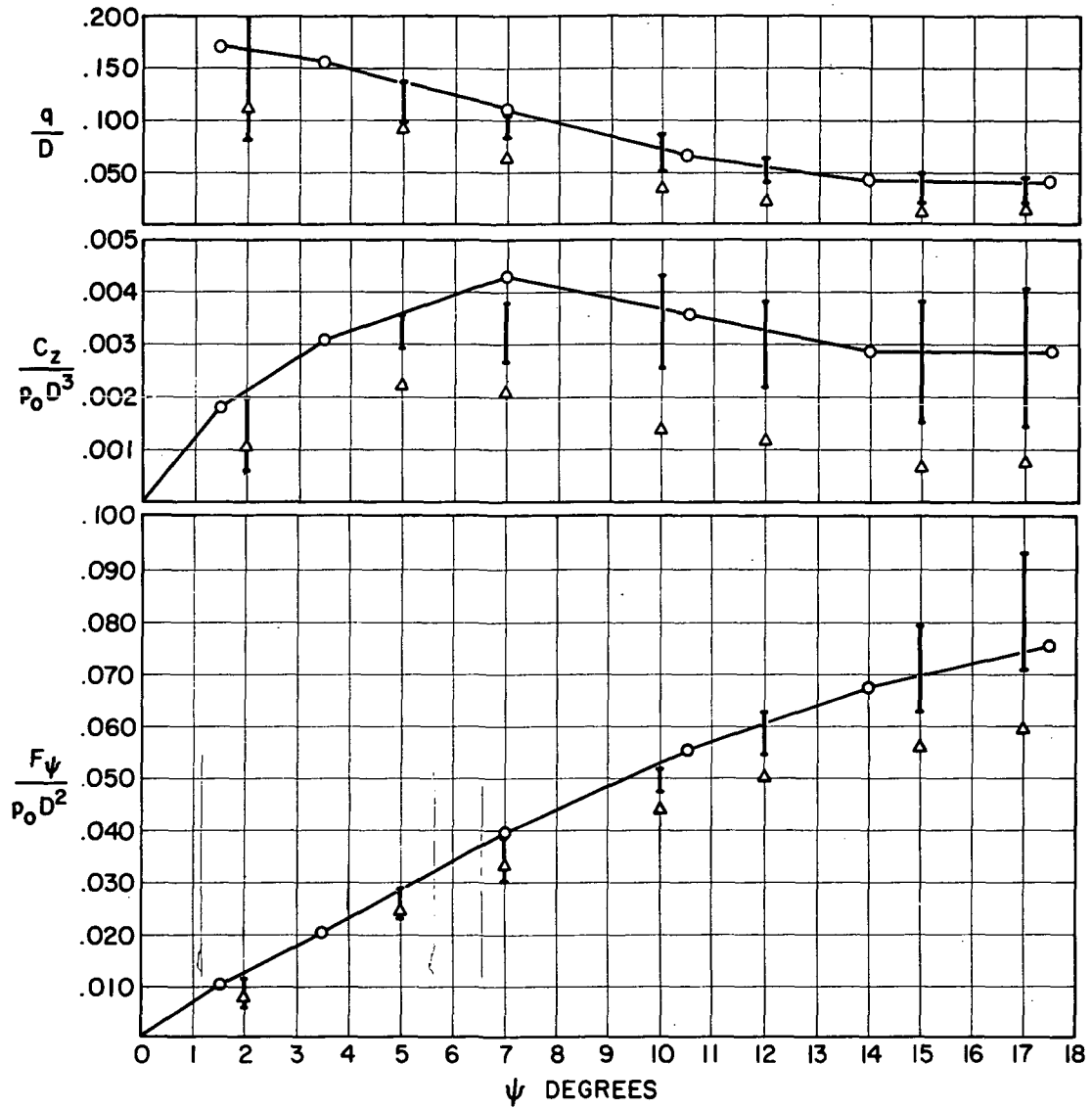
Figure 10. Yawed-rolling relaxation length
data for model and prototype tires.

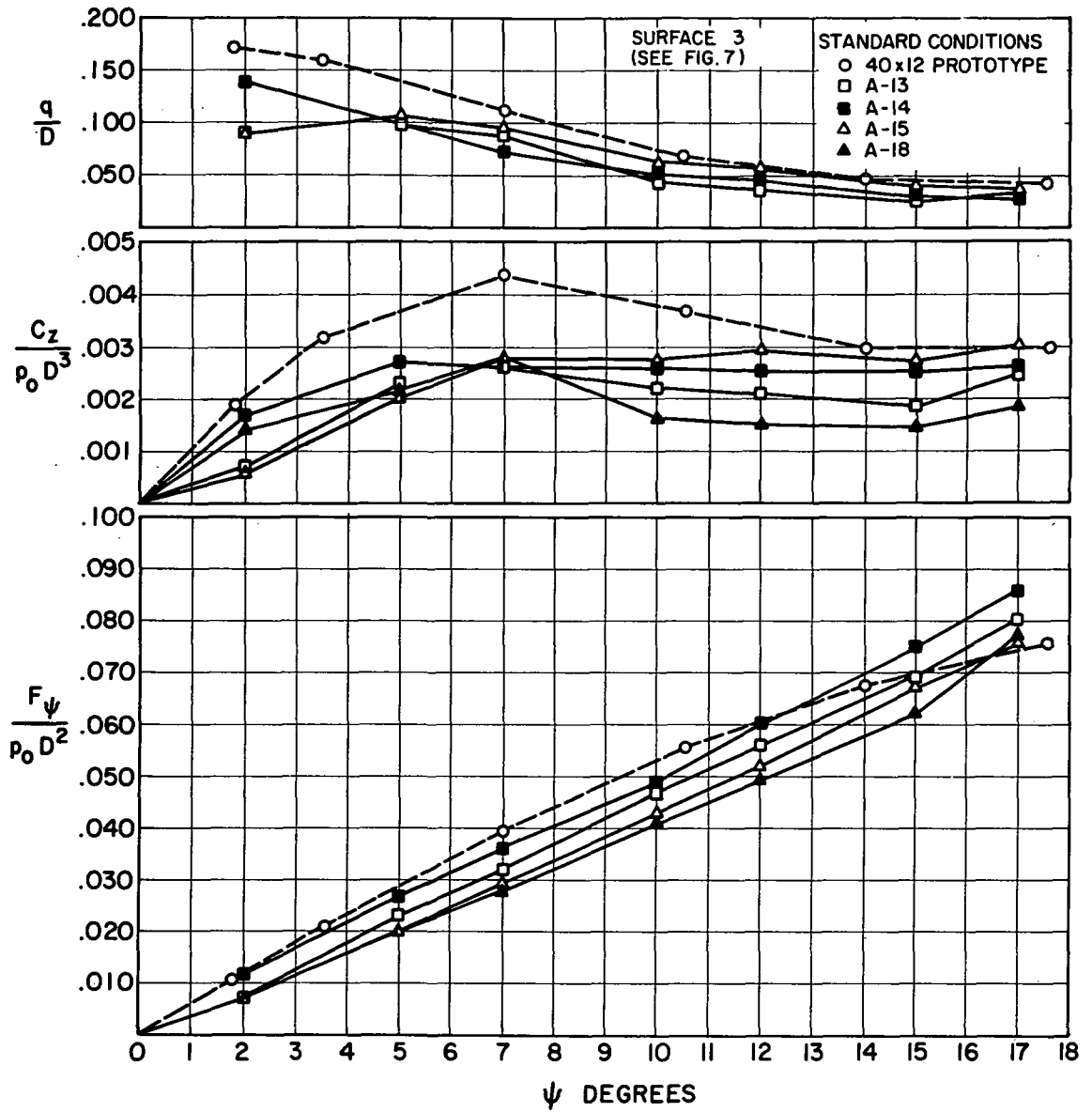Figure 11. Side force, self-aligning torque and pneumatic trail data for model and prototype tires. Surface No. 9.

Figure 12. Normal side force, self-aligning torque and pneumatic trail data for model and prototype tires. Surface No. 10.

A tire mechanical property which is also quite important in shimmy analysis is the tire lateral damping coefficient. Two comparisons between model and prototype tires for this property are shown in Figures 8 and 9. As can be seen, the agreement is very good in Figure 8, where the lateral damping coefficient is defined as the ratio of the maximum half-height of the corresponding force-deflection hysteresis loop to the maximum total force, as defined by Horne and Smiley [6]. The agreement is also good in Figure 9, where the lateral damping coefficient is alternately defined as the ratio of the energy loss per cycle to the energy contained in the area beneath the loading portion of the load-deflection curve.

An important tire rolling property used in shimmy analysis is the yawed-rolling relaxation length. This is defined as the distance a yawed tire must roll to produce a side force equal to $(1 - 1/e)$ of the maximum side force developed at the steady-state steer angle condition. A comparison of such measurements on the model tires with those taken on the prototype is shown in Figure 10. Again, agreement is good between the two sets of data.

There are two additional tire mechanical properties important to shimmy analysis which require a rolling tire for their definition. They are tire side force and self-aligning torque caused by operating the tire at various slip angles. These two properties were measured for the model tires used here, and from this measured data the pneumatic trail was gotten by taking the ratio of self-aligning torque to side force for a particular set of conditions. All three of these properties are presented in the subsequent graphs.

33

One important characteristic of these three tire properties is imme-
diately evident. This is their strong dependence on the type of surface on
which the tire rolls. A total of ten surfaces were used in the experimental
measurement of side force and self-aligning torque. The range of values
gotten from these tests is shown in Figure 11, where it is seen that the
spread of data is quite significant, and illustrates a strong influence of
surface conditions. Generally the full size prototype tire data lies inside
the ranges shown, with the exception of the peak self-aligning torque. This
is possibly lower in these model tests since they were done against a cylin-
drical roadwheel, while the prototype data was taken on the runway. Our
contact patch will generally be somewhat shorter and our pressure distribution
somewhat less favorable for developing peak self-aligning torque than the flat
runway surface.

Figure 12 shows this data for four model tires, and for the prototype
tire, for a specific roadwheel surface. There is some variation among the
model tires due to structural difference, particularly in the self-aligning
torque. However, this surface is not particularly the best one for model
tire mechanical measurements, and "sharper" surfaces, with more asperities,
may tend to reduce this scatter.

This entire comparison represents an interesting and we feel fruitful
observation, applicable in general to the determination of tire mechanical
properties, since it seems to indicate that different observers and experi-
menters can only expect complete agreement between tire mechanical property
data taken on identical runway surfaces. This clearly has application to
cooperative testing programs where various agencies participate.

MEASUREMENT OF STATIC LOAD-DEFLECTION PROPERTIES

All static load-deflection data was collected on what will hereafter be referred to as the Static Testing Device. This device was designed so that the model tire could be tested to obtain each of the four basic mechanical spring constants previously mentioned in this report, vertical load-deflection, lateral load-deflection, fore-aft load-deflection, and twisting moment-rotation.

Construction of the device is very simple, consisting of a wooden base, two steel loading plates, a tubular steel 90°-elbow arm, a rotating yoke, a steel point hinge, and a counterweight. Figures 13 through 17 show different views of a model tire under test in it. The bottom steel loading plate was attached to
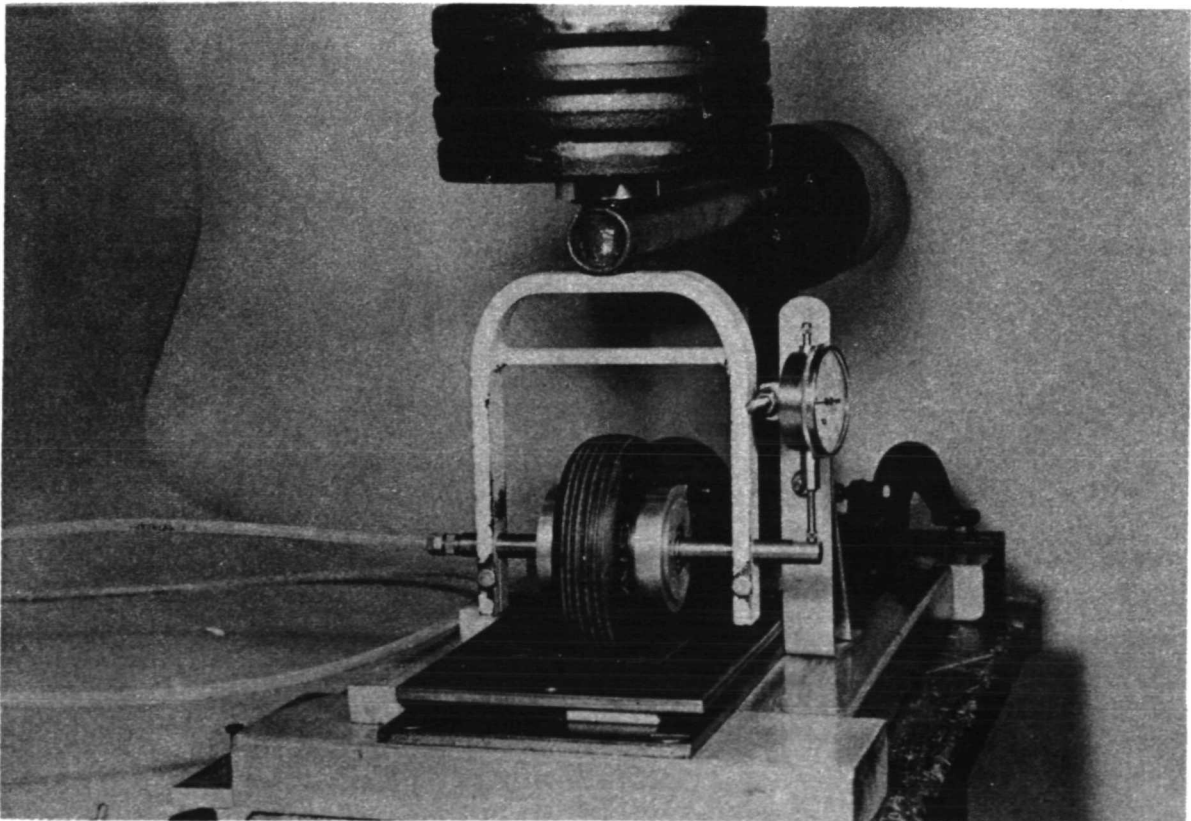
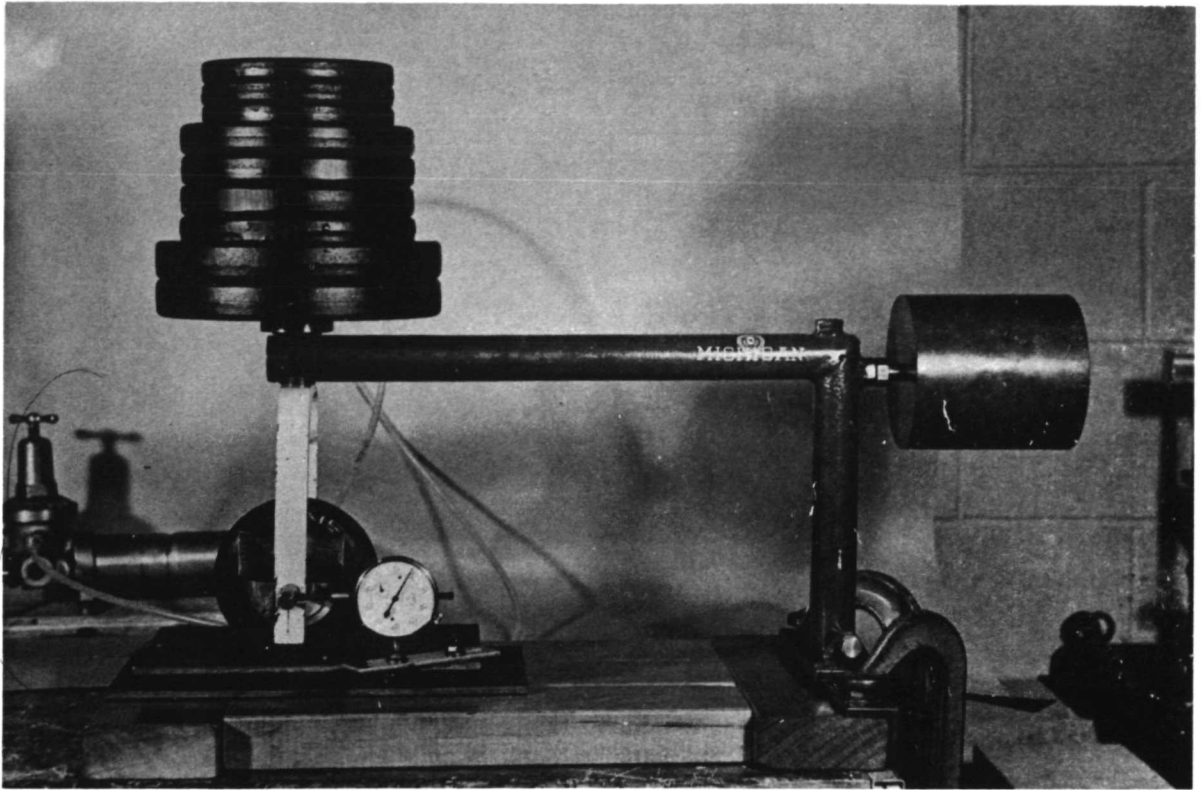Figure 13. Vertical load-vertical deflection test for model tire.

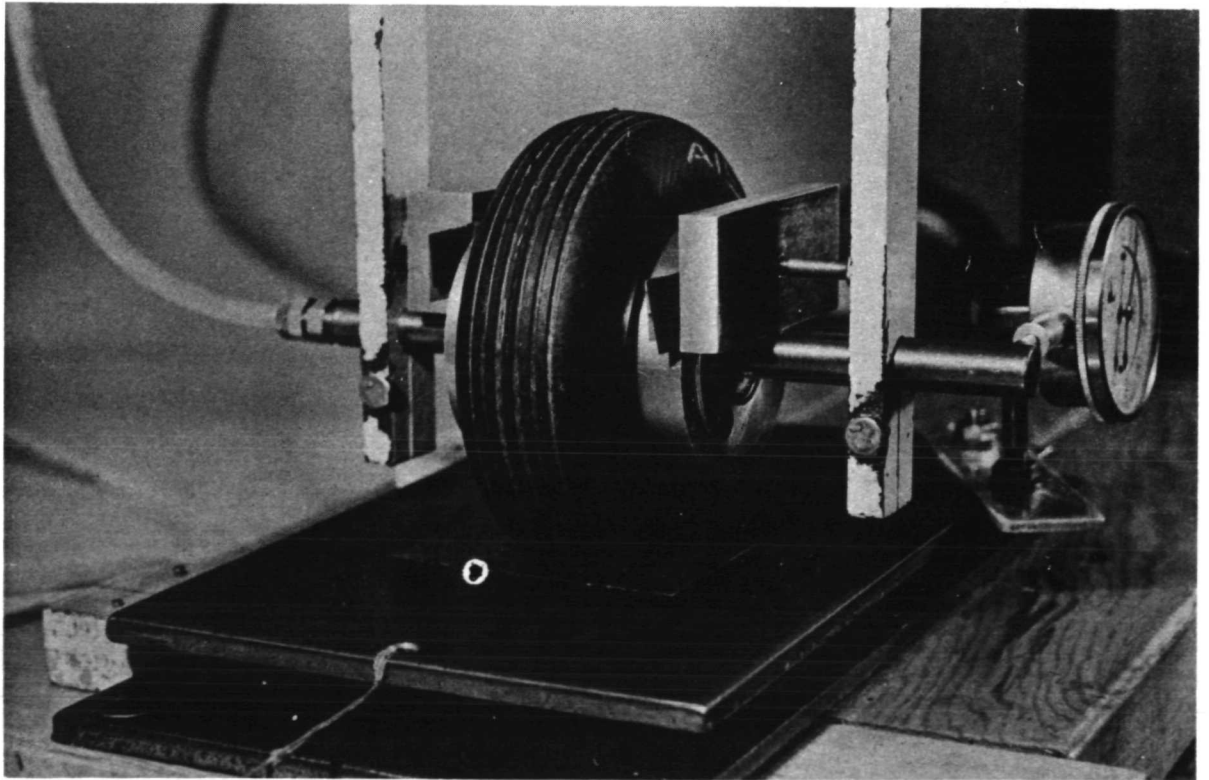Figure 14. Fore-aft load-deflection test for model tire.

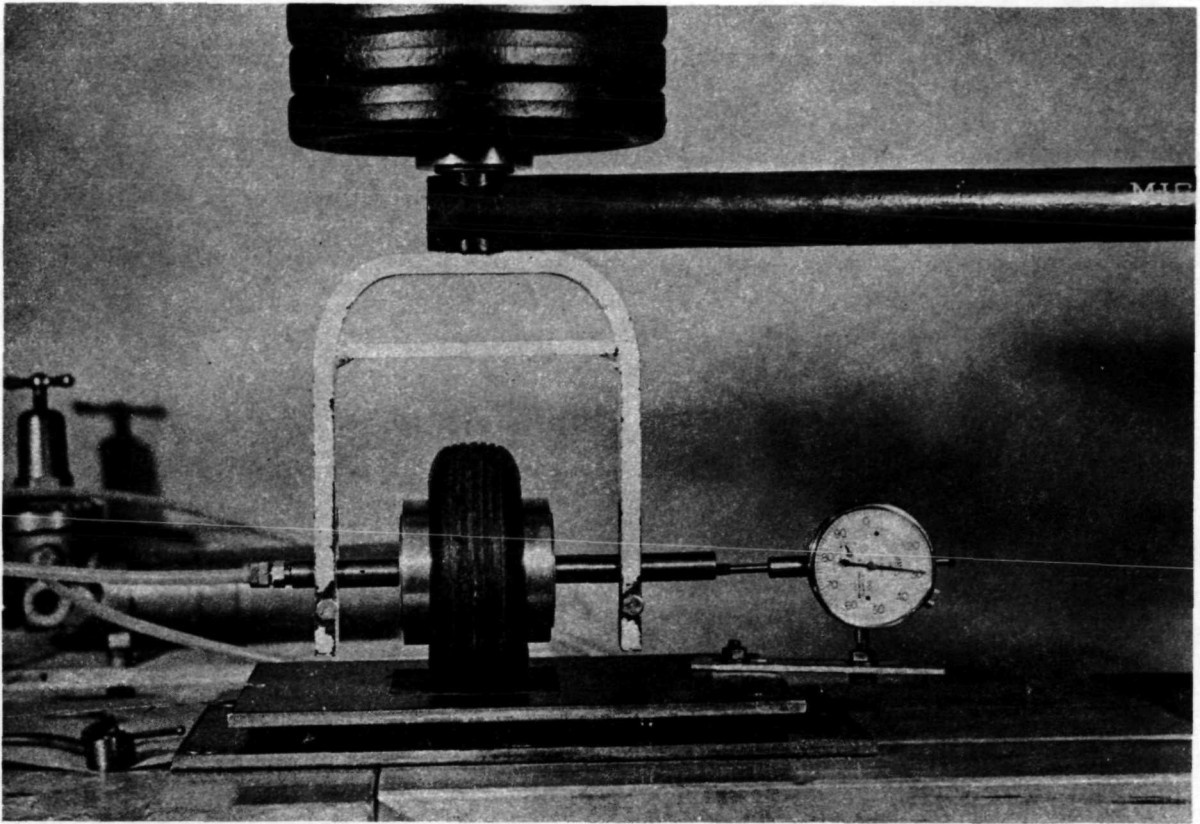Figure 15. Close-up of fore-aft test showing brake.

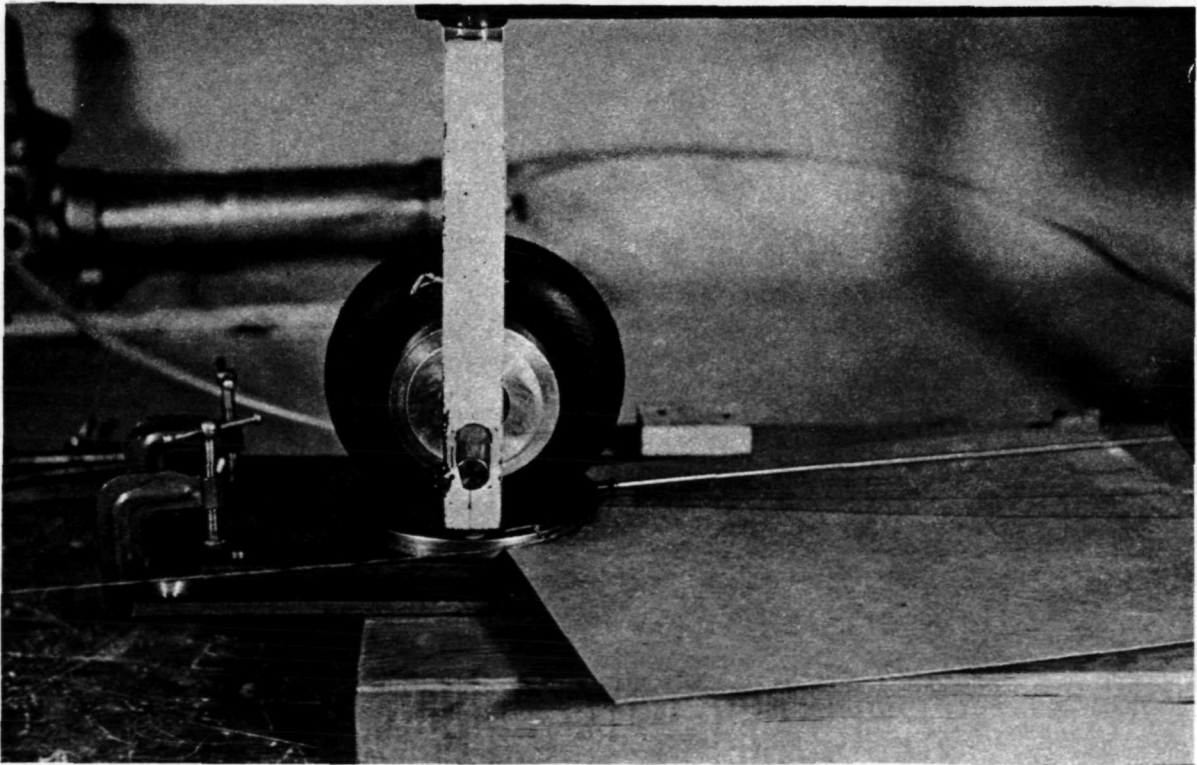Figure 16. Lateral load-lateral deflection test for model tire.

Figure 17. Twisting moment-rotation test for model tire.

the wooden base, and the top loading plate had three .437 in. dia. bearing balls sandwiched between it and the bottom plate. The top plate had a high friction surface bonded to it with contact cement so that tire slippage was held to a minimum during loading.

The tires were inflated through a small hole along the axis of the axle, opening into the interior of the rim with oil seals inserted within to maintain pressure. The pressure was regulated by a low-pressure regulator, which was monitored periodically so that proper pressure was maintained. Inflation pressures could be held to within ± 1/2 psi. with this regulator. It is important to have close pressure control in these experiments due to the large scale ratio, in this case 8.65.

Experimental reproducability was good for vertical load-deflection where, on the average, data could be reproduced to within ± 3%. For twisting moment-rotation, data variation was as high as ± 8%, and for lateral and fore-aft experiments, it was as high as ± 10%. To compensate for this, the tires were tested a minimum of three times and also rotated to a new position before each run. This amount of variation in properties is not particularly large, since studies on full size tires indicate a similar set of variations.

As a matter of record, all the deflection data collected was taken at "apparent equilibrium"; i.e., when all creep had ceased.

The first measurement on a model tire was that of its basic fore-aft spring rate, as previously discussed. This was generally done at a relatively high pressure (e.g., 20-25 psi). Then after obtaining $(k_x)_m$, Eq. (25) was used to calculate the reference pressure for the model tire:

38

$$(p_o)_m = \frac{(k_x)_m}{(k_x)_p} \cdot \frac{(D)_p}{(D)_m} \cdot (p_o)_p \tag{25}$$

Using the appropriate values for each of the variables the prototype, Eq. (25) becomes:

$$(p_o)_m = \frac{(k_x)_m}{(D)_m} \frac{(39.3)(95)\,(\cancel{in.})(\cancel{lb})(in.^{-2})\quad (lb)(\cancel{in.^{-1}})}{6800\quad(\cancel{lb})(\cancel{in.^{-1}})\,(\cancel{in.})}$$

$$(p_o)_m = .549 \frac{(k_x)_m}{(D)_m} \text{ psi} \tag{25a}$$

Using this calculated reference pressure, one may use $\Pi_7 = (\frac{F}{p_o D^2})$ to calculate the proper vertical load that should be used for the model tire to simulate the 14,500 lb rated load of the 40 x 12 prototype. This gives

$$(F_z)_m = (p_o)_m (D^2)_m \frac{14500}{(95)(39.3)^2} \text{ lb} \;,\; \text{or}$$

$$(F_z)_m = .0989 (p_o)_m (D^2)_m \text{ lb} \tag{26a}$$

For example, tire A-14 had a fore-aft stiffness $(k_x)_m = 160$ lb/in. From Eqs. (25a) and (26a), one would find that the reference pressure and vertical load should be:

$$(p_o)_m \simeq 19 \text{ psi}$$

$$(F_z)_m \simeq 39.8 \text{ lb} \;.$$

With these new parameters, a second fore-aft measurement would be made to verify

that the correct $(k_x)_m$ had been determined. When this had been done, then the other mechanical properties were measured and compared with the prototype.

It is worth listing some of the principles and techniques used in measuring the various mechanical properties:

(1) All loads applied to the contact patch in the xy-plane were applied away from the hinge of the static testing device to keep side movement of the hinge-arm to a minimum.

(2) The model tire was always relieved of vertical and side loads, i.e., allowed to relax in a free static position, a few minutes before proceeding with the next run for any particular test.

(3) The dial gauge was mounted between the moveable top plate and the axle to obtain both lateral and fore-aft deflections. Yoke and rim movement were observed to be negligible.

(4) The zero point for vertical deflection was defined as that point when the tire just touched the top loading plate.

(5) Inflated dimensions of the model tires were obtained by averaging readings taken at five places around the tire circumference. Both the width and diameter were measured directly.

MEASUREMENT OF GEOMETRIC AND SLOW-ROLLING PROPERTIES

STATIC PROPERTIES

Model tire footprints were taken by the ink and paper method at standard conditions of inflation pressure and vertical load. The contact length was measured from the footprint. Figure 18 shows a typical footprint.

**STANDARD
CONDITIONS**

INCHES

Figure 18. Typical model tire footprint.

Lateral damping cycles were taken on the apparatus shown in Figures 19 and 20. This apparatus basically consists of the static testing device discussed in the previous section. Here the lateral force is generated by a lead screw and transmitted through a strain ring force-transducer to the movable plate. The plate rests on three steel balls and translates with almost no friction. The plate displacement relative to the rim of the tire is measured by a LVDT inserted between the tire yoke and the plate. Both displacement and
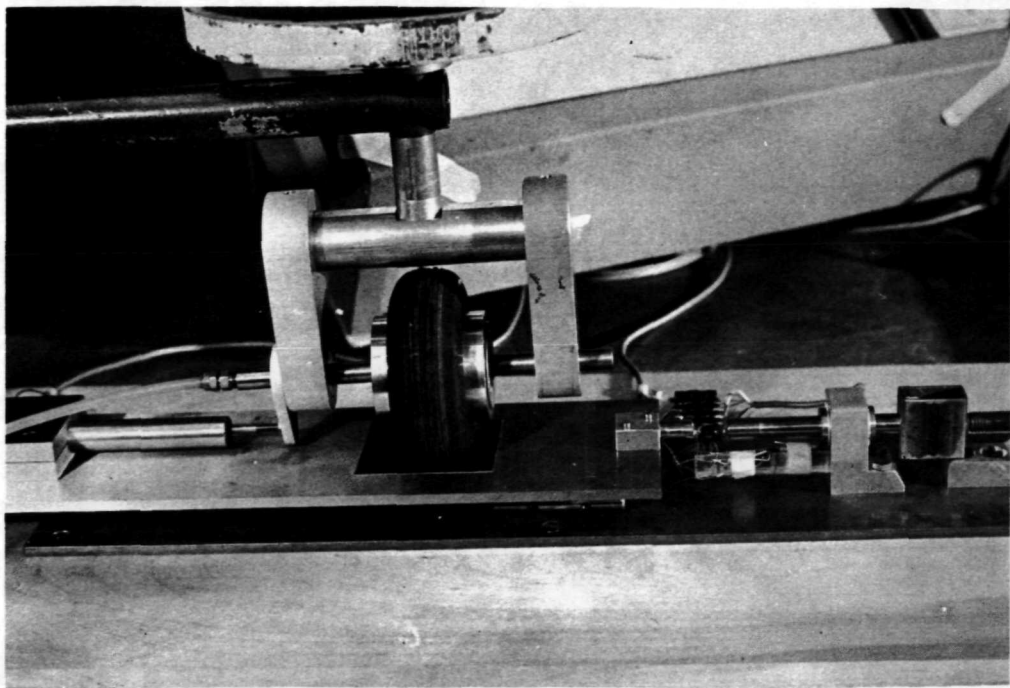
41

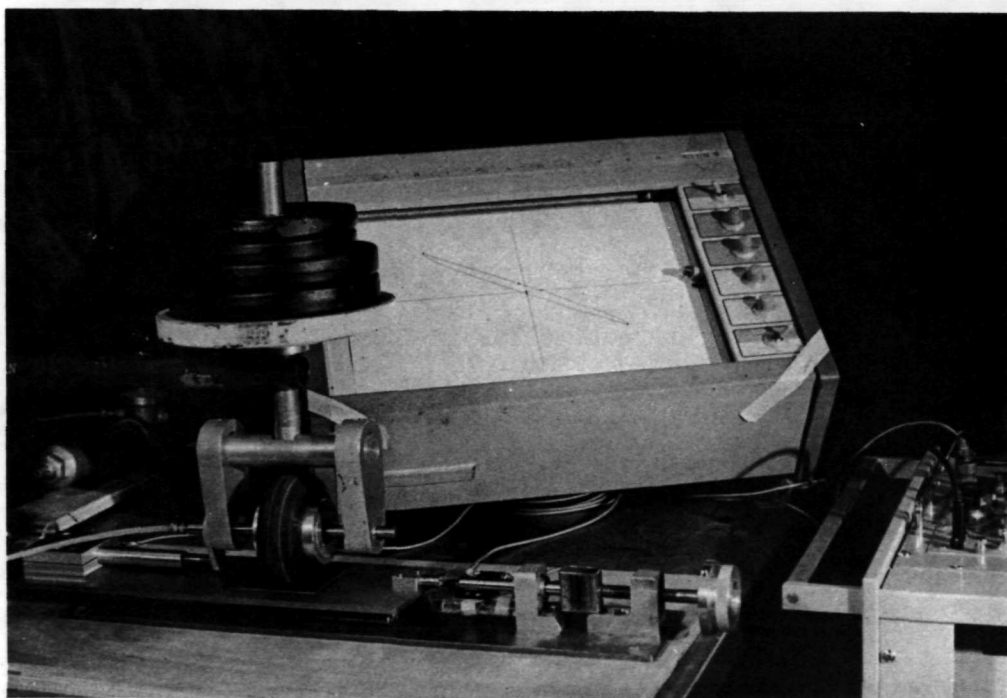Figure 19. Components of lateral damping test apparatus.

Figure 20. Lateral damping test apparatus.

force signals are fed into Sanborn carrier amplifiers with the outputs of the amplifiers going into an X-Y recorder. Figure 19 shows the movable plate, tire and transducers. Figure 20 shows an overall view of the testing machine, Sanborn recorder and amplifiers and the X-Y recorder.

A typical lateral hysteresis loop is shown in Figure 21. Because of the dimensionless nature of most damping coefficients, no scales are needed for the axes. One definition of a lateral damping factor, used by Smiley and Horne [6], is the ratio of the maximum half-height of the force-deflection hysteresis loop to the maximum total force. Referring to Figure 21, $(\eta_y)_F$ is equal to the ratio A/B of the forces. Another definition of damping factors is based on energy or area measurements. The definition used in the preceding section is the ratio of the energy loss per cycle to the energy per cycle defined by the triangular area under the top curve. Referring to Figure 21, $(\eta_y)_E$ is equal to the ratio of the areas $\Delta E/E$.

SLOW ROLLING PROPERTIES

The slow rolling tests were performed on a 30-in. diameter, 4-in. wide cast iron roadwheel. Different adhesive surface are attached to the polished cast iron surface to simulate different roadways. The tire and rim assembly are mounted in a yoke such that forces normal to the plane of the wheel and moments about the vertical axis can be measured. The yoke is mounted in bearings attached to the end of a horizontal hinged arm, so that the whole assembly can easily be swung up off the roadwheel and out of contact. The roadwheel, yoke and arm are shown in Figure 22. The normal or side force, F_ψ, is measured by a strain ring force transducer shown in Figure 23. The

43

LATERAL
FORCE , F_y

LATERAL
DEFLECTION

δ_y

ΔE

E

2A

A

B

$(\eta_y)_F = \dfrac{A}{B}$

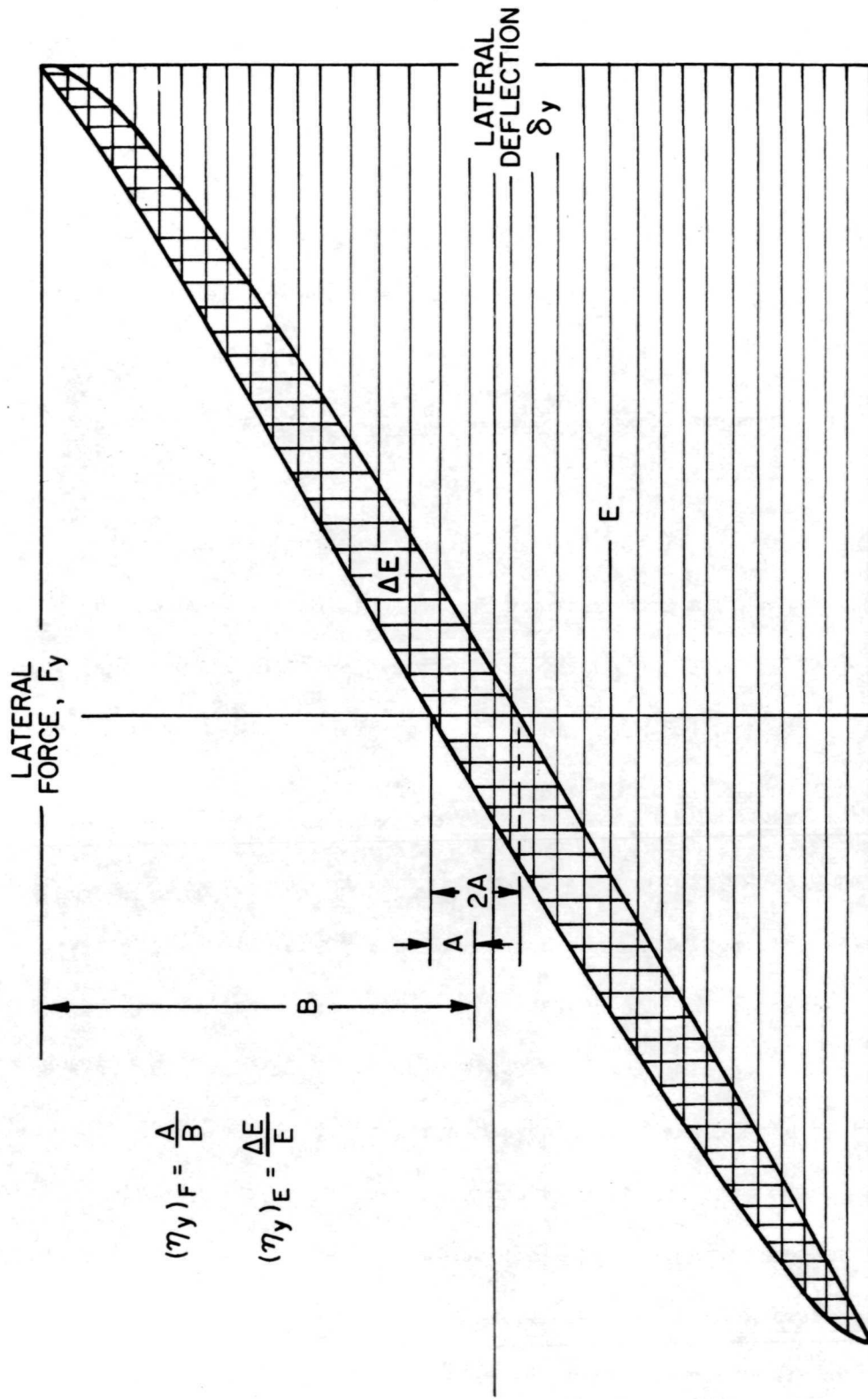$(\eta_y)_E = \dfrac{\Delta E}{E}$
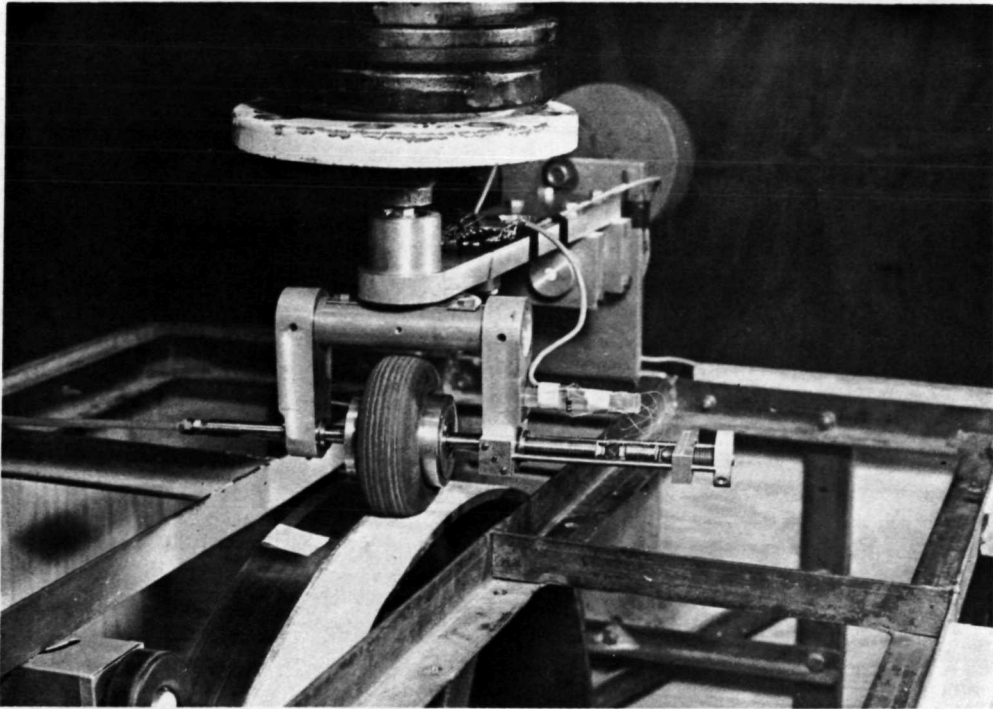
Figure 21. Typical lateral hysteresis curve.

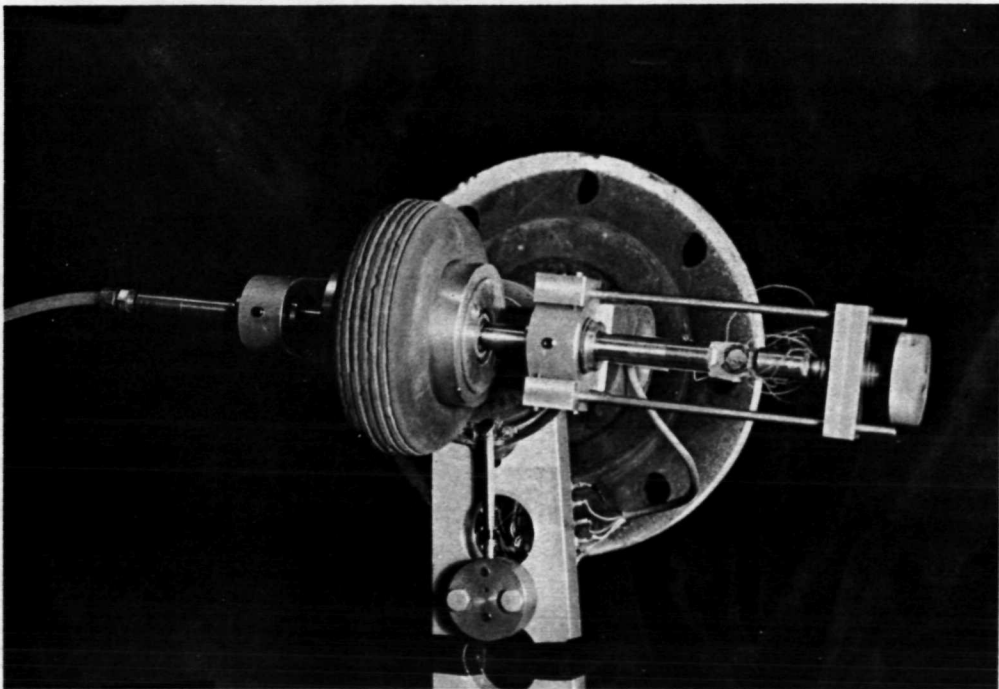Figure 22. Model tire roadwheel, yoke and arm assembly.

Figure 23. Transducers for measuring
side force and self-aligning torque.

model wheel bearings are mounted in the rim so that the non-rotating axles can be mounted in linear ball bushings and attached to the force transducer. The force transducer butts against a rigid harness attached to the yoke and measures side force perpendicular to the wheel plane. The torque C_z about the vertical axis is measured by a drag link transducer shown in Figure 23. The yoke is mounted in ball bearings to allow rotation about the vertical axis. A drag link with a built-in end at the arm and a pin joint at the yoke is instrumented with strain gages. The pin joint is attached to a slider which can be clamped at the desired yaw angle.

Relaxation length, λ_y, was measured by placing the tire at a yaw angle, rotating the roadwheel one tire contact length and measuring the side force build-up. The roadwheel displacement is measured by a precision potentiometer circuit. The tire side force measurement is accomplished by the strain ring. Both roadwheel displacement and side force are recorded by an X-Y plotter, as shown in Figure 24.
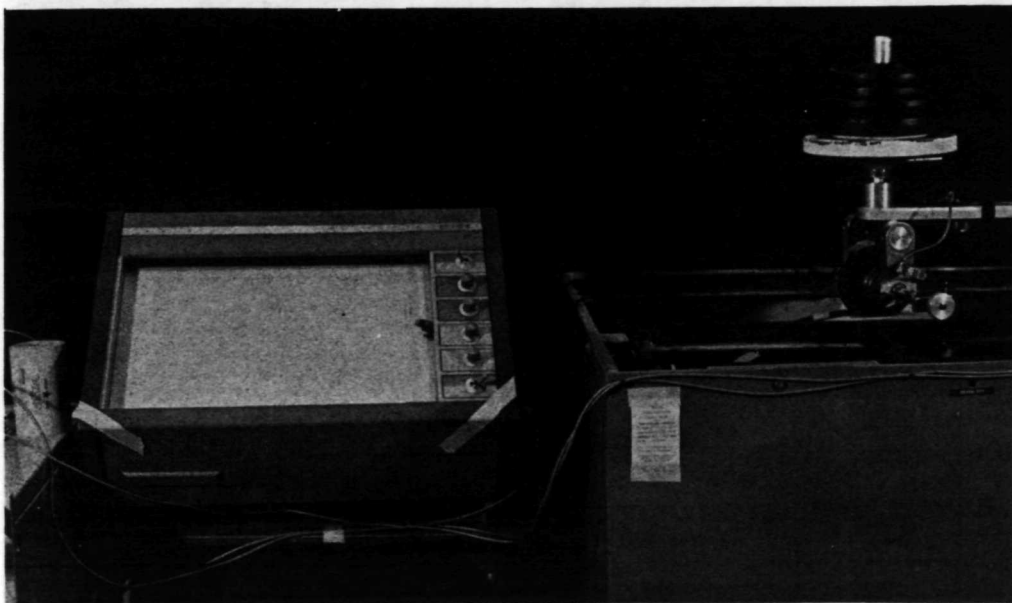

Figure 24. Yawed-rolling relaxation-length test apparatus.

46

Figure 25 shows a typical side force build-up curve obtained by this system. The tire rotates one contact length, $2l$, the axle and force transducer rest against the rigid harness and the side force build-up is recorded. The first horizontal slope is taken as the maximum side force. Variations after this point are due to maximum side force variation around the circumference of the tire. As shown in Figure 25, the maximum amplitude A is multiplied by $(1 - 1/e) = .632$. The distance the tire rolls to produce a side force of $.632A$ is the measured relaxation length, λ_y. A few tests using self-aligning torque in place of side force gave basically the same relaxation lengths.

Three other slow rolling quantities were measured on a steady state basis. Side force, F_ψ, self-aligning torque, C_z, and pneumatic trail, $q = C_z/F_\psi$, were measured while the roadwheel was rotated by hand at a speed of about 0.8 ft/sec. Figure 22 shows the test in progress. An individual procedure for finding zero yaw angle was used on each tire, and allowed it to be located to within $1/4°$. Once zero yaw angle is known, the tire was run at increasing yaw angles while the steady state values of F_ψ and C_z, were recorded on an oscillograph. Variations in these quantities, which at small yaw angles could be very significant, were usually due to circumferential tire structure variation and difference in tire mounting. To eliminate the effect of these variations, the average value was computed using three measurements taken in one direction of rolling. Then the tire was dismounted, turned around and the procedure duplicated. Then averages of both sides of the tire were averaged together to get the values used in the preceding section. Figure 26 shows
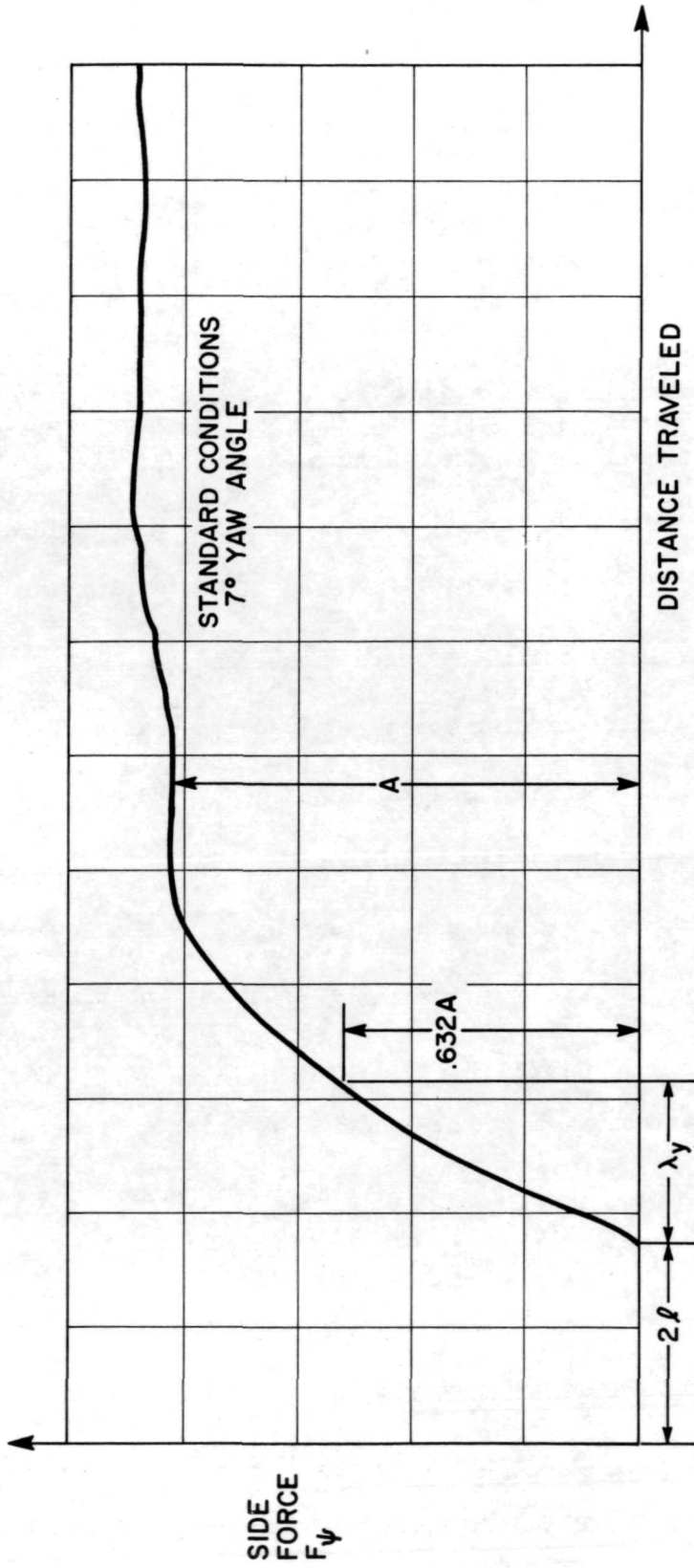
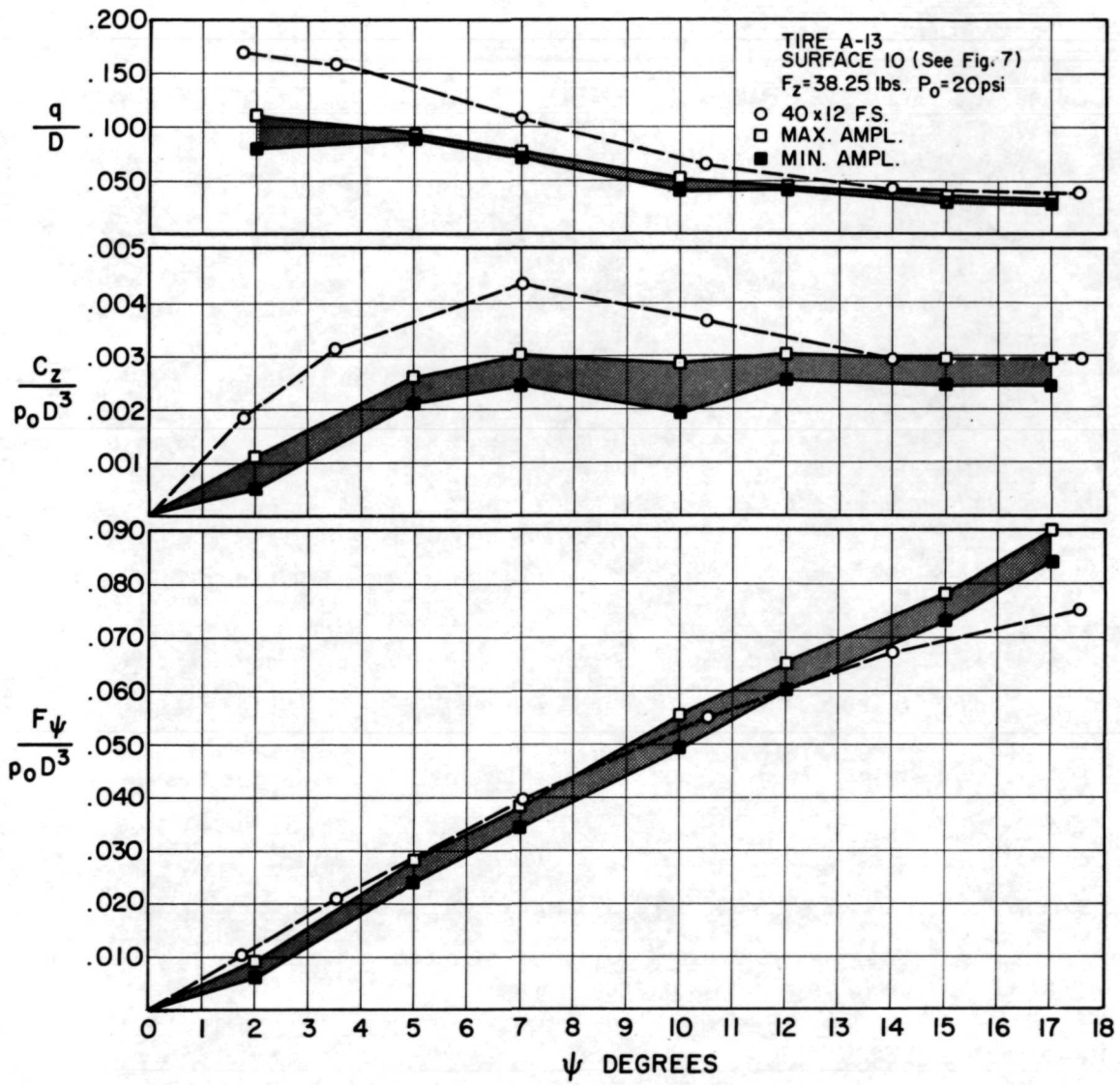Figure 25. Typical data and data reduction for determining yawed-rolling relaxation length.

48

Figure 26. Variations in side force and self-aligning torque due to circumferential variations of model tire.

the circumferential side force and self-aligning torque variation for one side, while Figure 27 shows the variation in maximum amplitude from one side of the tire to the other.

Another important variation in these three slow rolling properties is due to roadwheel surface variations, as previously discussed. Many different kinds of surfaces were tried. Figure 11 shows the variation in maximum amplitude due to ten different surfaces. Rough surfaces, such as sandpaper, Safety Walk and Safety Walk coated with dental stone, gave high forces and moments at high yaw angles and tended to abrade the tires. Smooth surfaces, such as clean cast iron, Scotch Tread and Scotch Tread coated with dental stone, gave low forces and moments, but did no apparent damage to the tire. Compromise surfaces, such as Safety Walk coated with Rox and dental stone, gave the highest forces and moments which did not damage the tires. It is these smoother surfaces which were used to obtain the data in the preceding section.
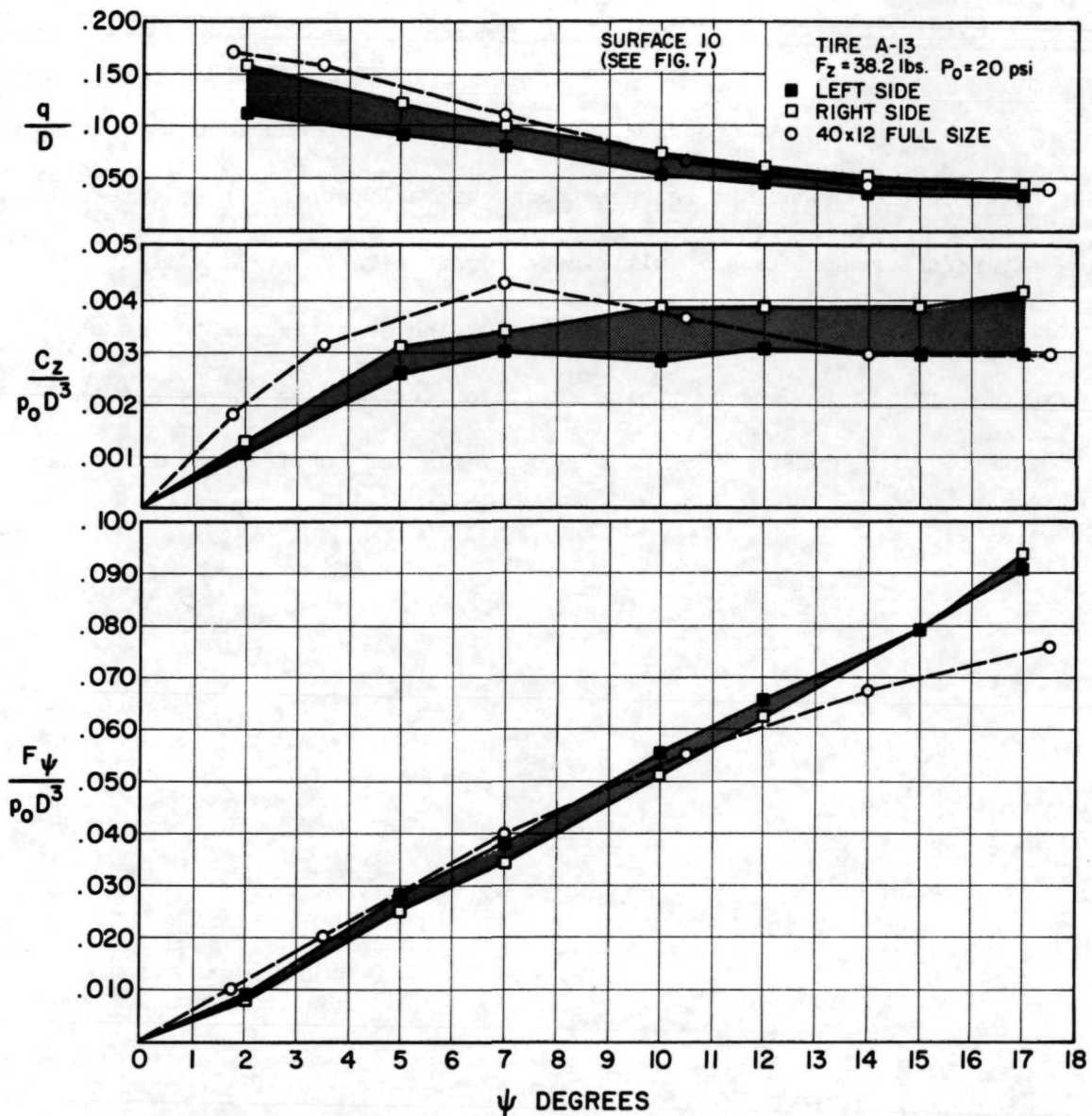
Figure 27. Variations in side force and self-aligning torque caused by side to side variations of model tire.

CONCLUDING REMARKS

The research program described in this paper has produced data showing that good correlation exists between the mechanical properties of carefully made aircraft tire models and full size aircraft tires. It is anticipated that this correlation could be useful in studying such diverse topics as shimmy of aircraft landing gear, the action of anti-skid systems, and the influence of tire construction and design variables on tire operating characteristics.

APPENDIX

MODEL TIRE CONSTRUCTION AND DEVELOPMENT

GENERAL COMMENTS

The initial model tire experiments were carried out with a commercial
Veco model airplane tire of 4.5 in. diameter. These experiments demonstrated
the general feasibility of small scale tire modeling, but also exposed serious
shortcomings in the Veco tire. These tires tended to creep, or grow with time,
so that their dimensions and mechanical stiffness properties changed slowly.
They had no cord structure, and so did not truly represent the elastic pro-
perties of an aircraft tire. Since scale modeling was our objective, it ap-
peared necessary to find ways of obtaining or making a model tire similar in
structure to a real tire.

Experiments showed that it was possible to form a small cord-structure
tire of model size using an inflatable bladder, similar to commercial tire
practice. Equipment was manufactured or purchased for making such tires.
The most important elements of this equipment were:

(a) A loom for hand winding tire carcass fabric, with provision for
variable cord end count. This is shown in Figure 28.

(b) A mold frame, or holder, in which the actual tire molds are in-
serted, and which serves to hold the two mold halves tightly to-
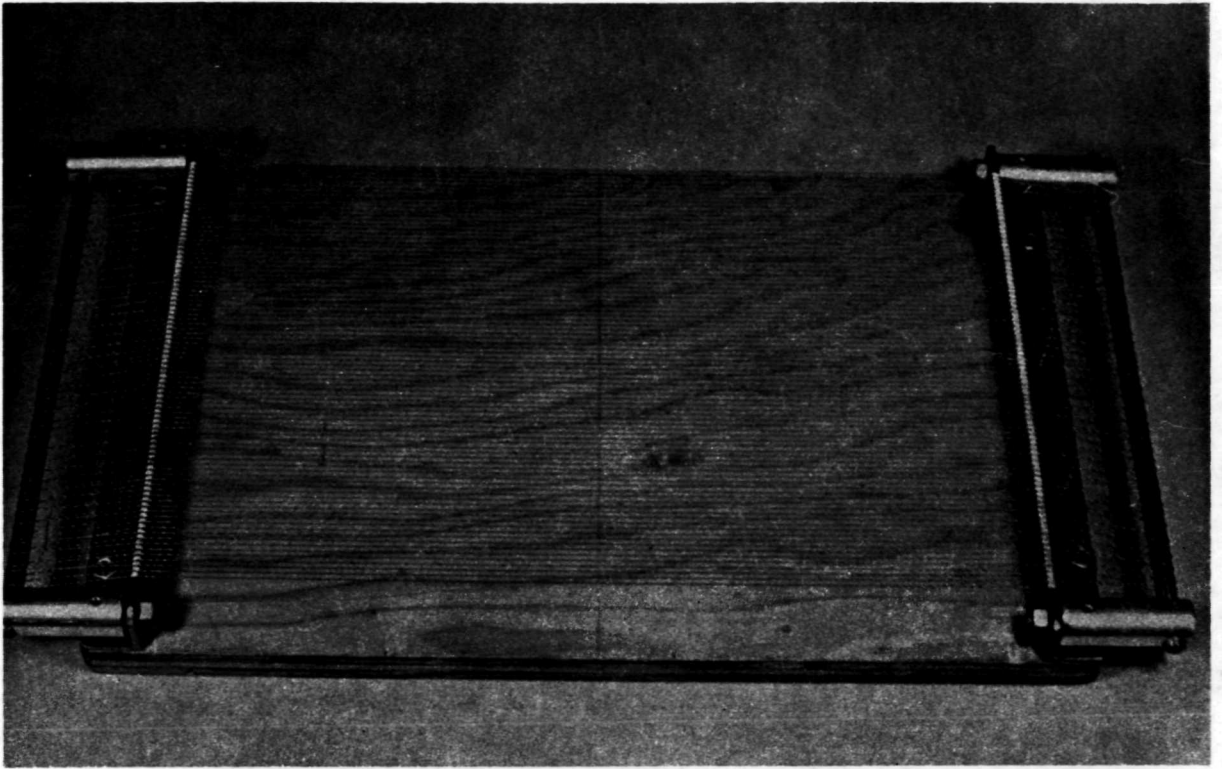gether. This is shown in Figure 29.

Figure 28. Loom for stringing tire cord.
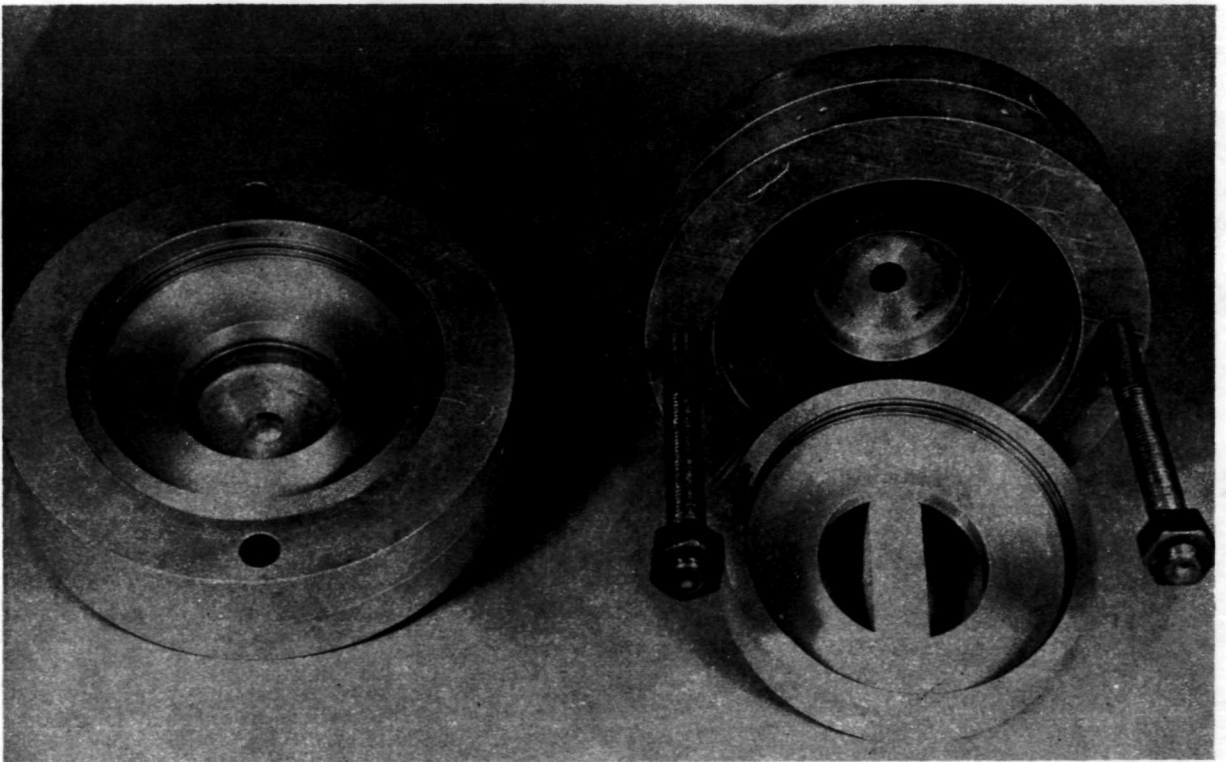

Figure 29. Mold inserts and holder.

(c) A tire mold, which forms the outer surface of the tire as also shown in Figure 29.

(d) A bladder for forming the tire against the mold.

(e) A laboratory oven for curing the tire.

The materials used for these tires were conventional tire cord, dipped into an adhesion promoter, and unvulcanized rubber sheet stock.

The bead of a tire is an area where considerable hand work is done in fabricating a commercial, full size tire. It did not appear possible to be able to duplicate bead constructions readily in small scale tires, nor did it seem particularly important to do so since the bead does not enter into any of the mechanical properties of the tire. These considerations led to a choice of a beadless tire design, which greatly simplifies tire construction and molding but at the expense of a somewhat more complicated wheel and rim. This is because the rim must now center, locate and grip the tire, functions which normally are at least in part performed by the bead. Figure 30 shows the rim with a dismounted tire. This rim has two side caps which screw inward and clamp the tire against a flange, one side cap being shown separately on the right hand side of Figure 30, along with its spanner.

Using this rim design, inflation is carried out through one hollow axle, which is stationary, while the wheel is mounted on the axle with bearings and seals. Leakage is minimal. This design allows various force transducers to be built into the nonrotating axle without the use of slip rings.

SCALE MODELING OF 40 x 12 TIRE

The 40 x 12 14 PR Type VII tire was chosen as a specific prototype since
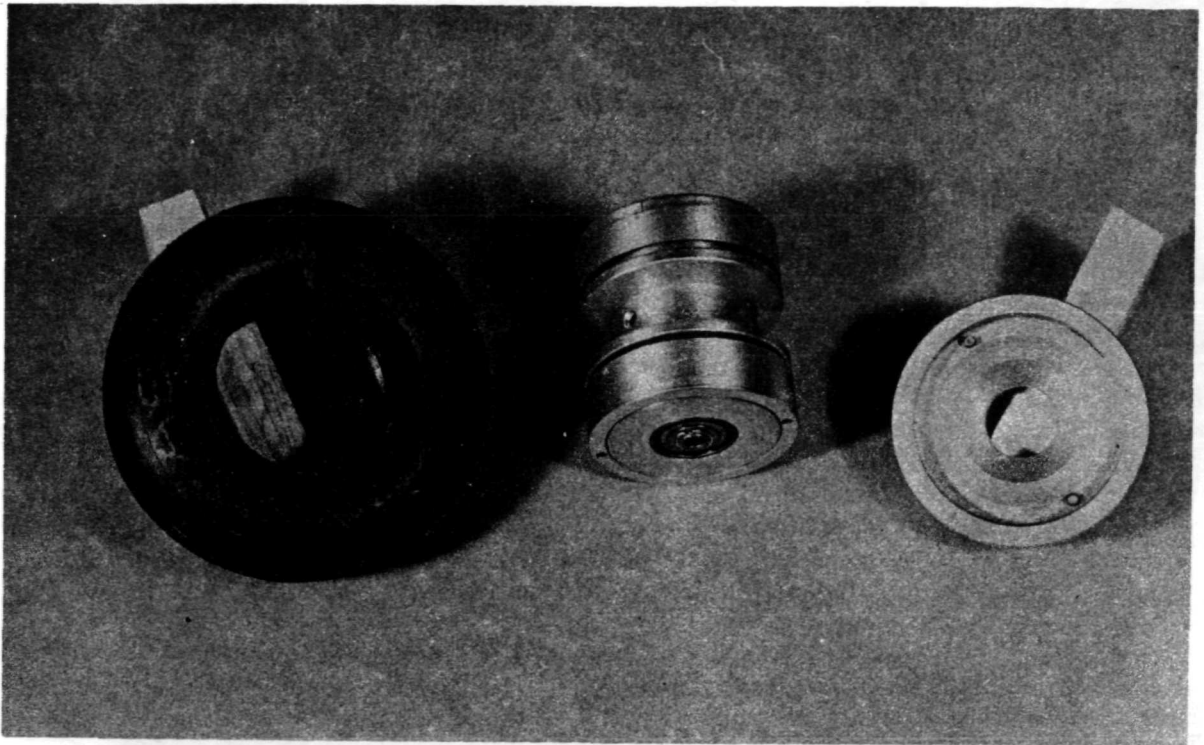
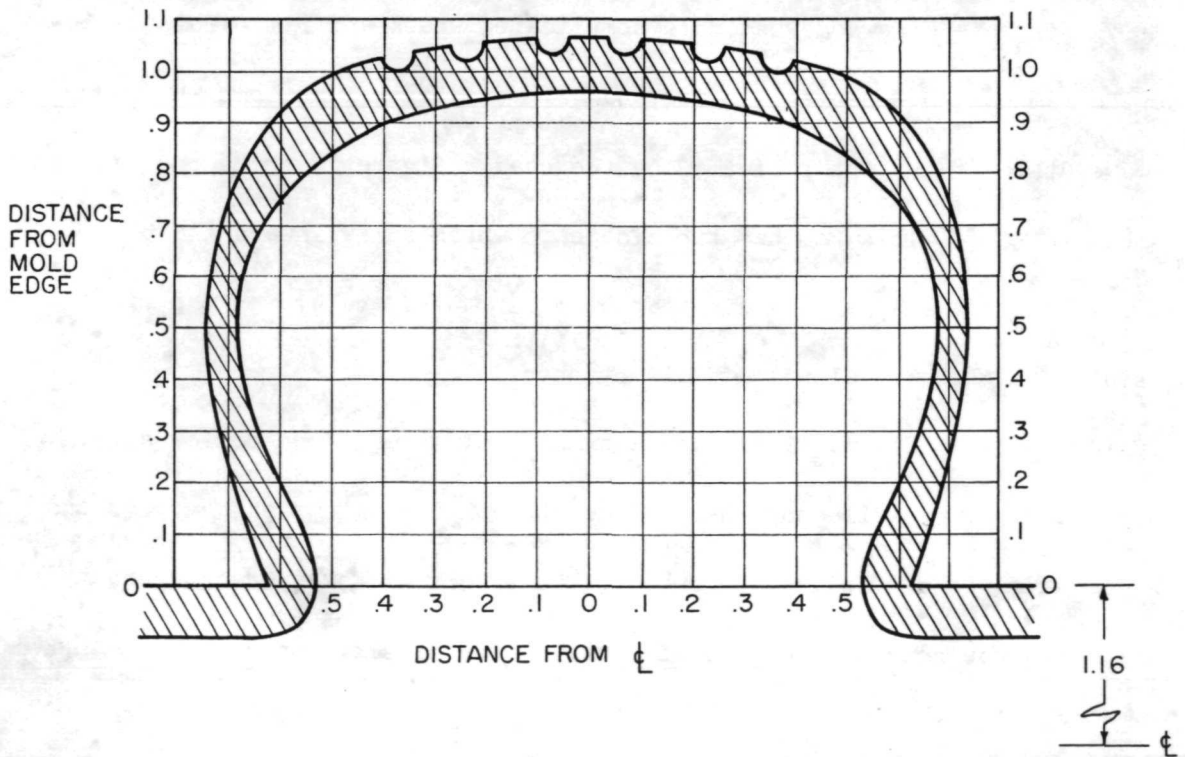Figure 30. Unmounted model tire, rim and spanner for dis-assembly.

Figure 31. Mold and tire cross-section for model of 40 x 12 tire.

it had been the subject of extensive mechanical property measurements by Horne and Smiley [6]. The mold was designed to be geometrically similar to the deflated outside cross-section of this tire, but with additional section height as dictated by the beadless design. Figure 31 shows the mold contour used. The mounted section height would, of course, be geometrically similar due to the presence of the rim flanges. Table I in a previous section shows the inflated dimensions of the model tires to be approximately correct, although model tire widths tend to be slightly high.

Molds were contour machined from aluminum, and wire inserts used to form the tread grooves.

The first step in building a model tire is writing a specification sheet. This is done so that a permanent construction record is available. A typical specification sheet is given in Table II for a two ply bias tire.

Next, cord must be selected and the tire carcass fabric made up. Three different cords were tested during this development, these being:

(a) An 840/2 nylon, which is the most common cord now used in full size aircraft tire construction

(b) One strand of the two-stranded 840/2 cord

(c) A single strand from a three strand special elastic cord. The single strand had a strong helical winding set, and exhibited a very low modulus

Of these three, it was found that the full 840/2 nylon cord appeared to be most adequate, and is further desirable since it is readily available commercially.

TABLE II

SPECIFICATION SHEET FOR TIRE A-14

Ply Stock: Cord - 840/2 nylon dipped cord
Rubber - .012" USR on each side
Loom - 10 cords/inch
Green cord angle - 60°
Ply width - 6-5/8"

Green Tire:

No. of pieces		Location	Width x Thickness	Rubber
(1)	Liner			
	1	on ₵	2-3/4" x .024"	BFG soft
	2	5/8" from ₵	5/8" x .024"	BFG soft
(2)	Ply 1			
(3)	Separator			
	1	on ₵	6-5/8" x .024"	BFG soft
	1	on ₵	2" x .024"	BFG soft
(4)	Ply 2			
(5)	Tread			
	2	3/4" from ₵	3/8" x .024"	BFG soft
	1	on ₵	2-1/2" x .024"	USR
	2	1-7/8" from ₵	1/2" x .024"	USR

Final Width - 6-1/2"

Bladder - made from bicycle tube

Curing:
2:40 PM	~80°F		in oven	
3:40 PM	270°F	} 1/6		
3:55 PM	300°F	} 1/3		
4:10 PM	320°F	} 1/2		
4:25 PM	320°F	} 1/4		
4:33 PM	320°F	}	out	

The first step of the actual construction is the fabrication of the ply-stock. The loom is strung as previously shown in Figure 28. A cord count of 10 ends per inch was chosen for the model tires used in this report, since two plies of this material are approximately equal in elastic stiffness to one ply of the actual tire fabric used in the prototype tire. A thin sheet of unvulcanized rubber is laid on either side of the parallel cords, as shown in Figures 32 and 33 and is rolled down tightly. The completed ply fabric is then cut to the proper bias angle as shown in Figure 34.

The tread, liner and separator rubber pieces are cut to size, as given in the specifications, from unvulcanized rubber sheet of the proper thickness.

As shown in Figure 35, a two-inch tube mounted in a metal-working lathe serves as the building drum. The tube is covered with Saran Wrap to allow the green tire to be removed easily after building. Typical is the layup of tire A-6. First, a rubber liner is rolled on and stiched down, shown in Figure 36. Then ply 1 is rolled on, Figure 37, followed by ply 2 and the first layer of tread, Figure 38. Finally, after the tread is completed, a tread cover is rolled on with the lathe knurling tool, Figure 39. The green tire cylinder is then cut to desired length and labeled with a silver ink pen, which when cured, leaves a permanent identification marking. Figure 40 shows the finished green tire flanked by the mold inserts.

The tire is now ready for molding and curing. First the tire is covered with talcum powder which serves as a mold release agent. The bladder is then made ready by stretching it over its tapered end plugs, and is then inserted into the uncured tire. This is shown in Figure 41. The most successful bladders
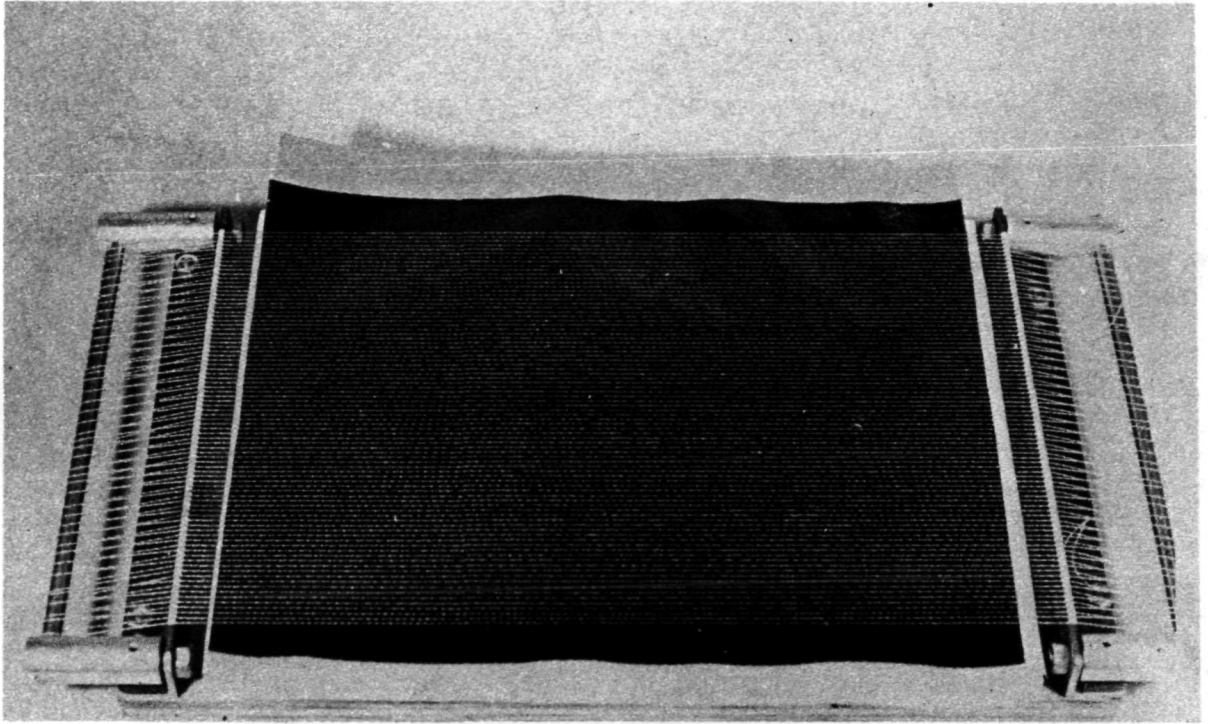
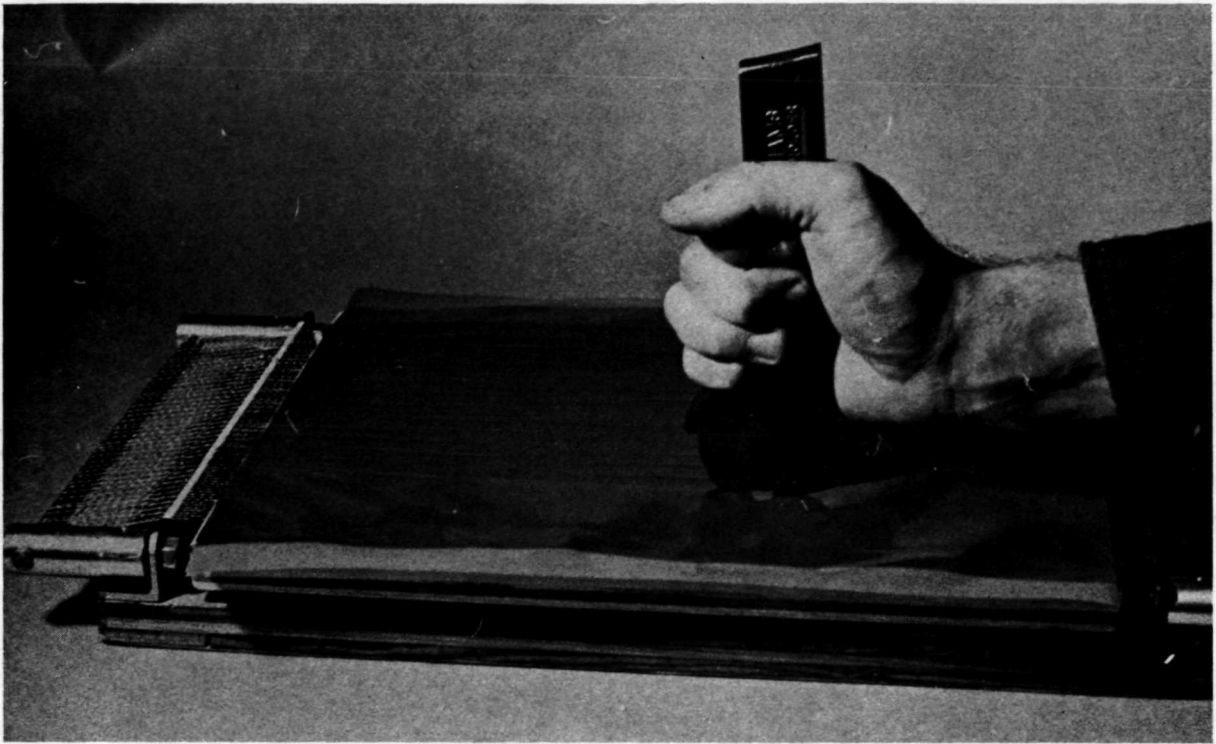Figure 32. First step in rubberizing the tire cord.
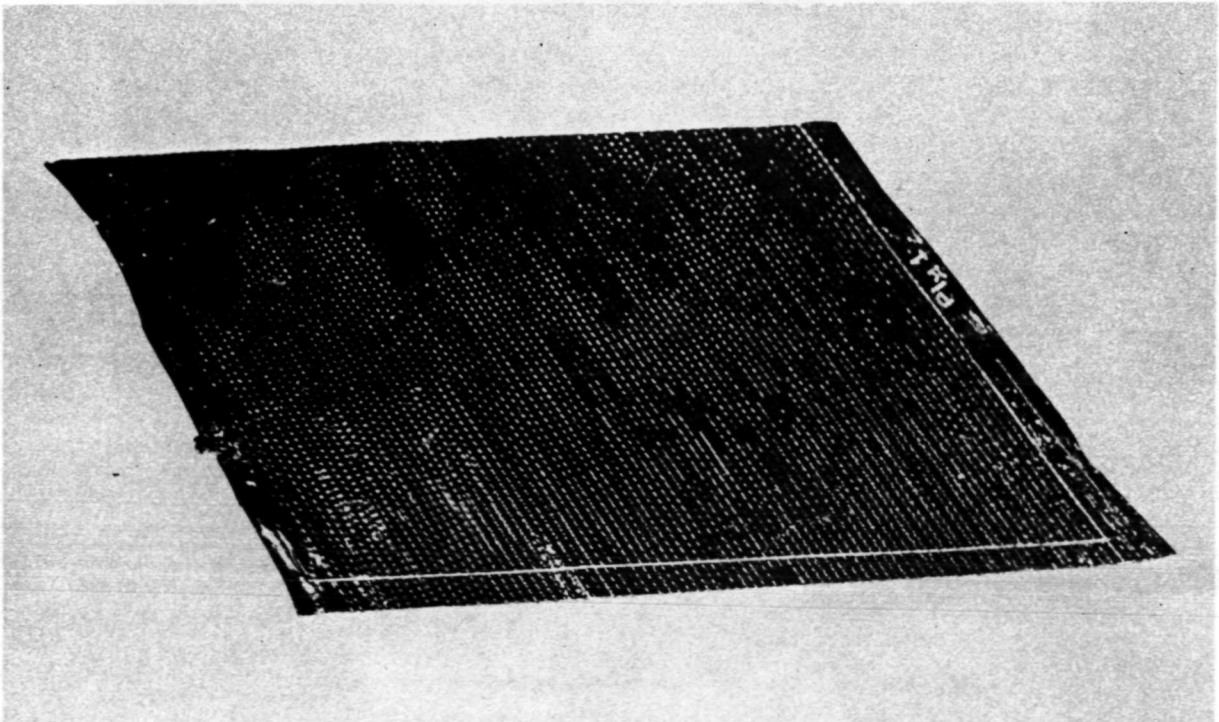
Figure 33. Completing the rubberized fabric.

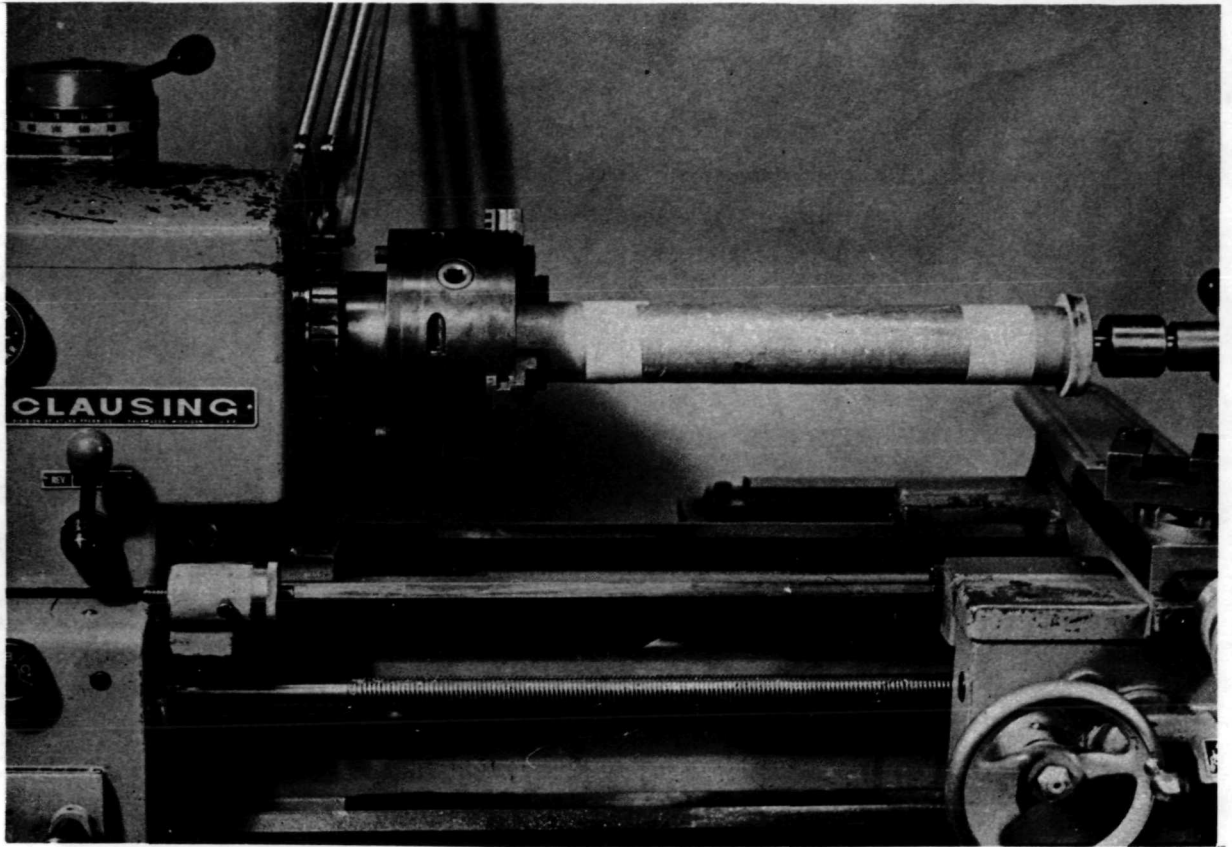Figure 34. Finished fabric cut to a bias angle.

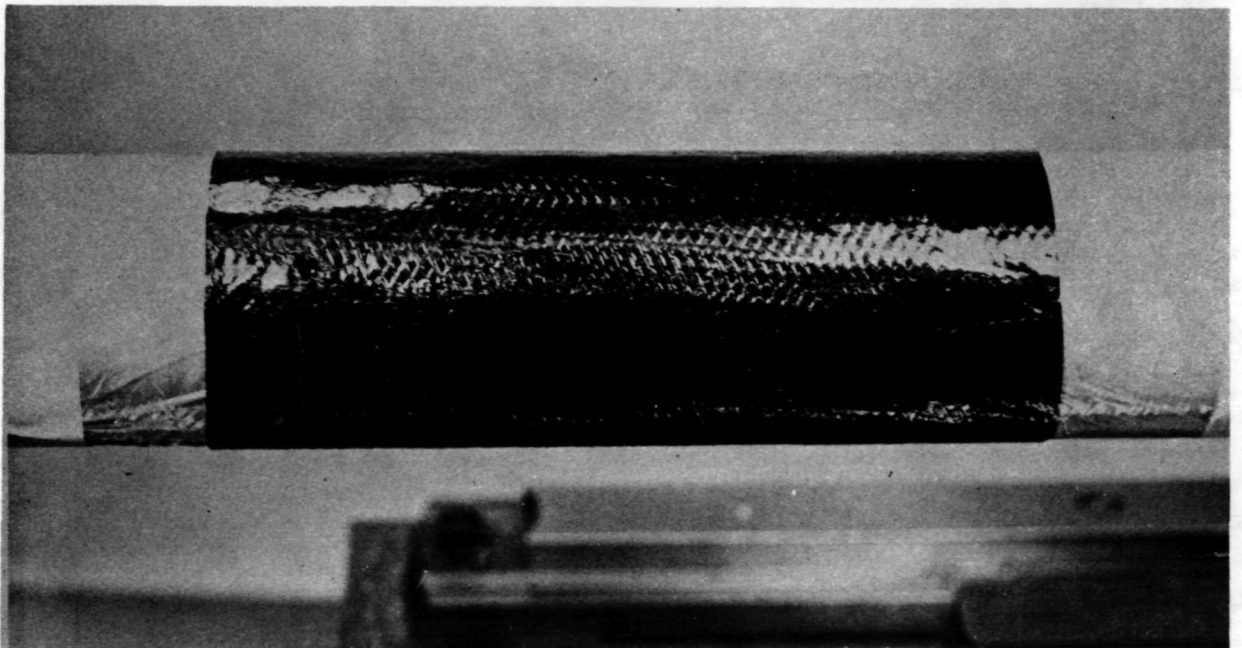Figure 35. Mandrel for laying up the tire.

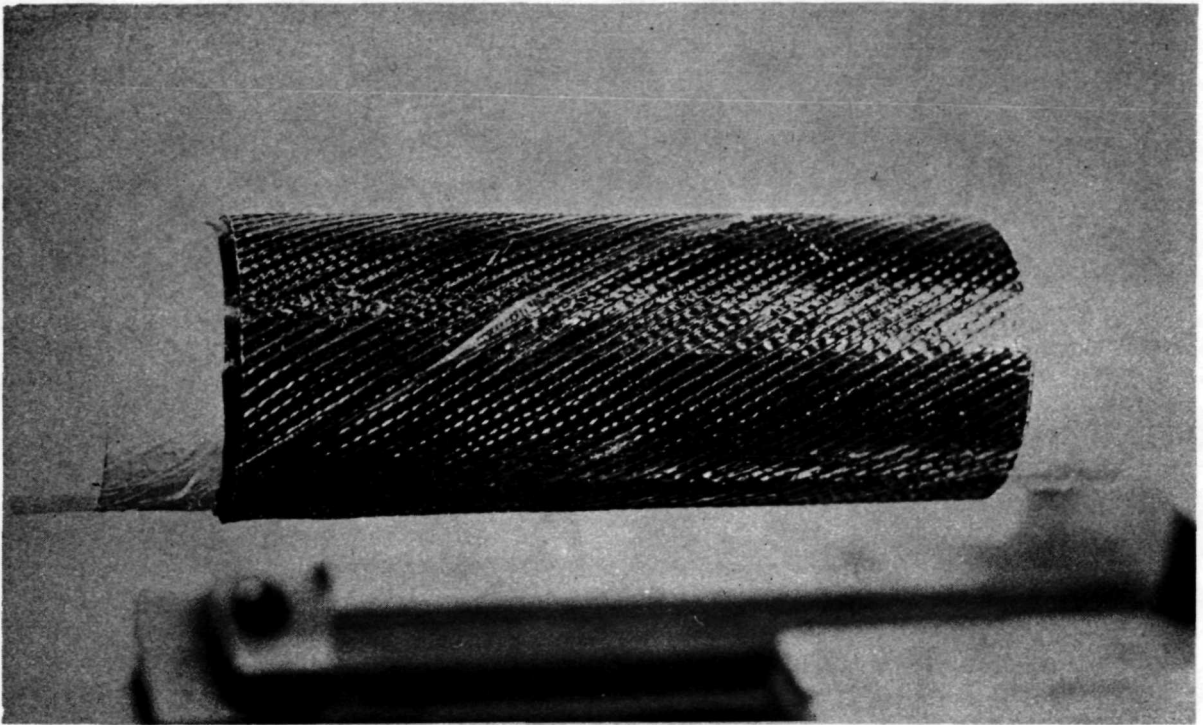Figure 36. Rubber liner on building drum.

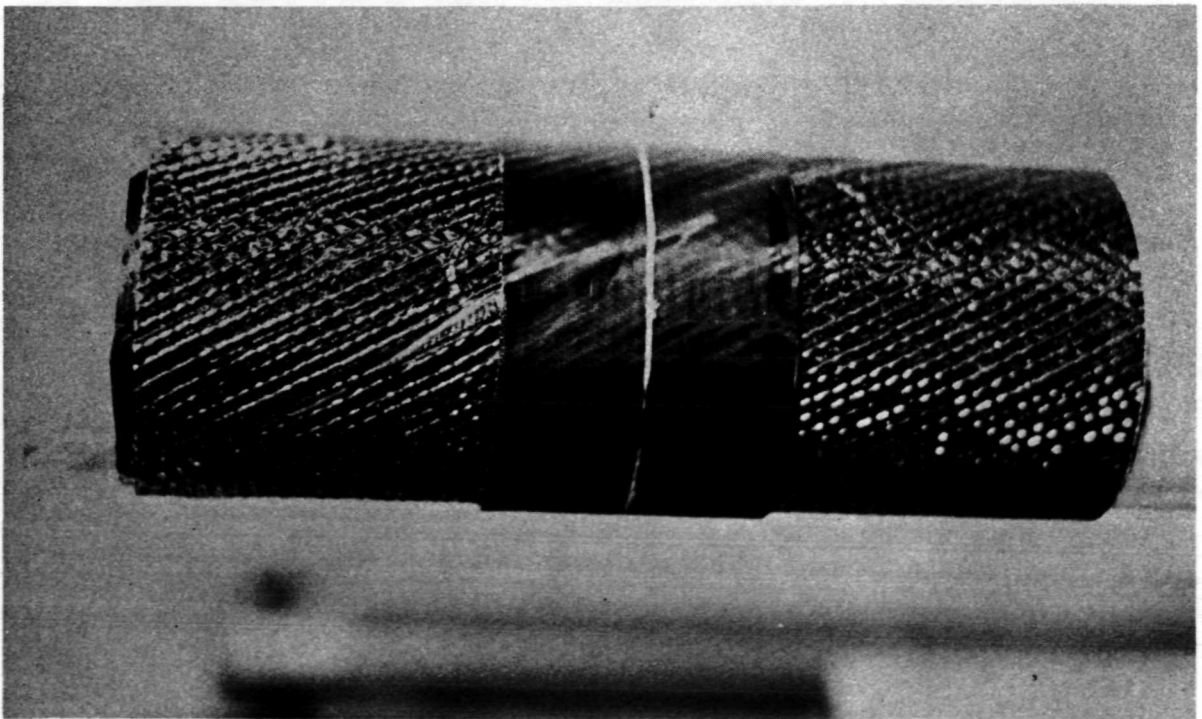Figure 37. First ply of fabric on building drum.

Figure 38. Ply 2 and tread on building drum.

63

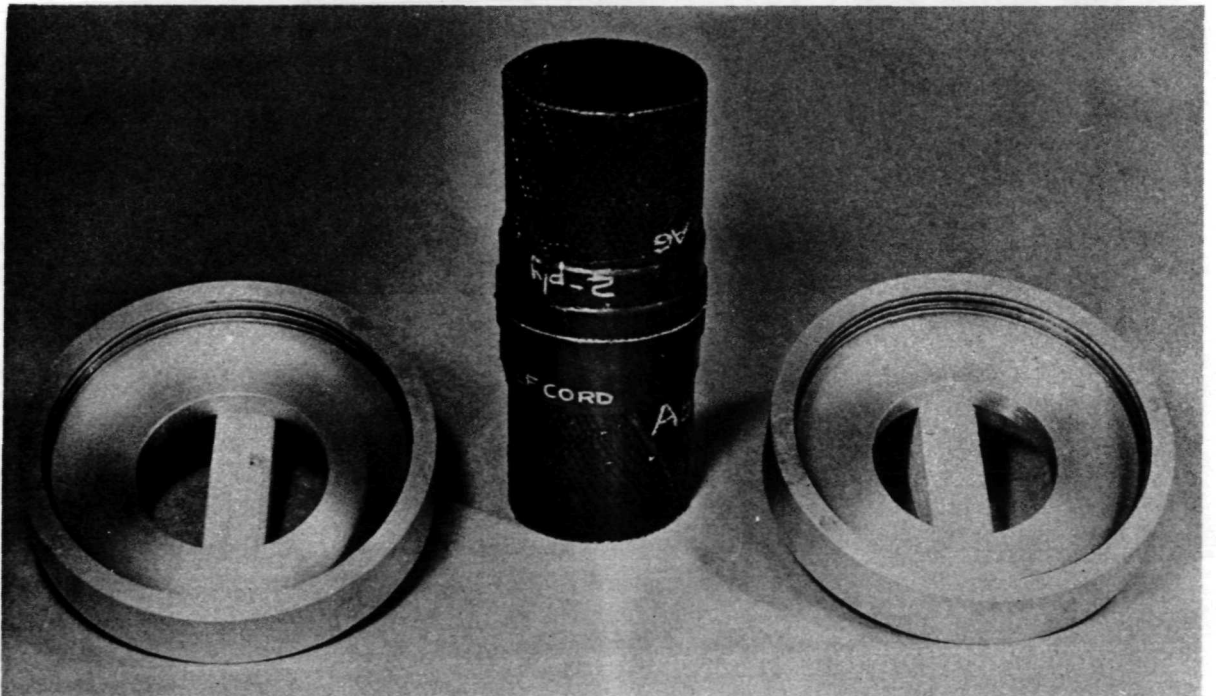Figure 39. Rolling on the tread cover.

Figure 40. Completed green tire and mold inserts.
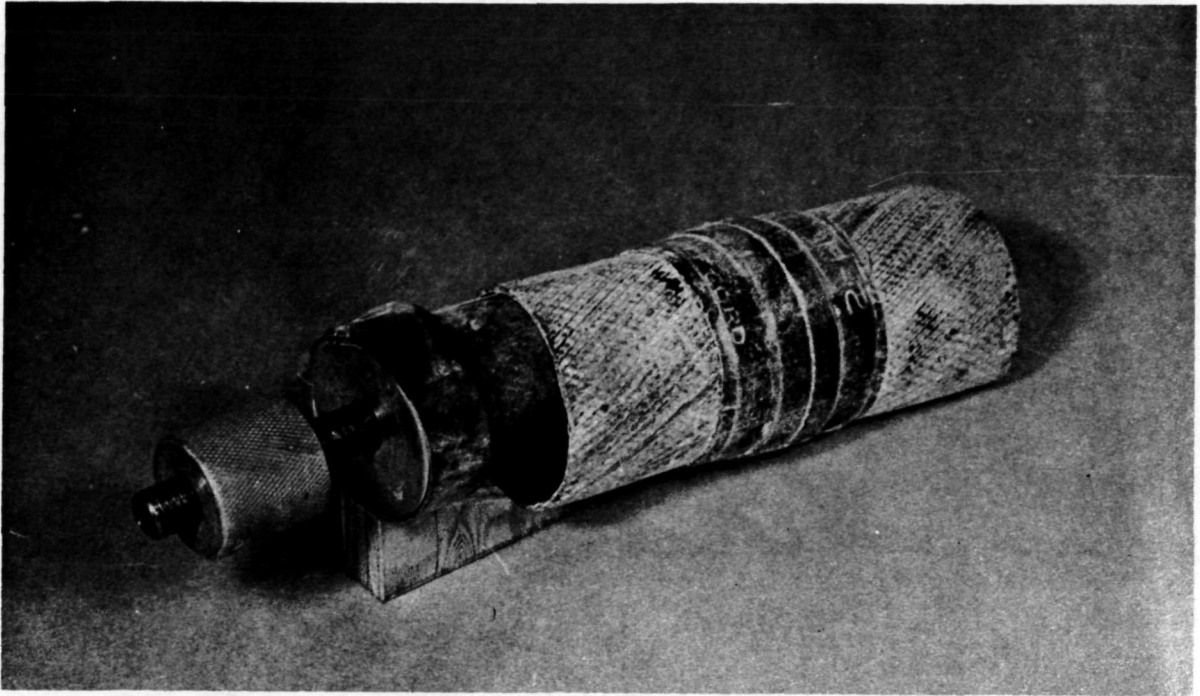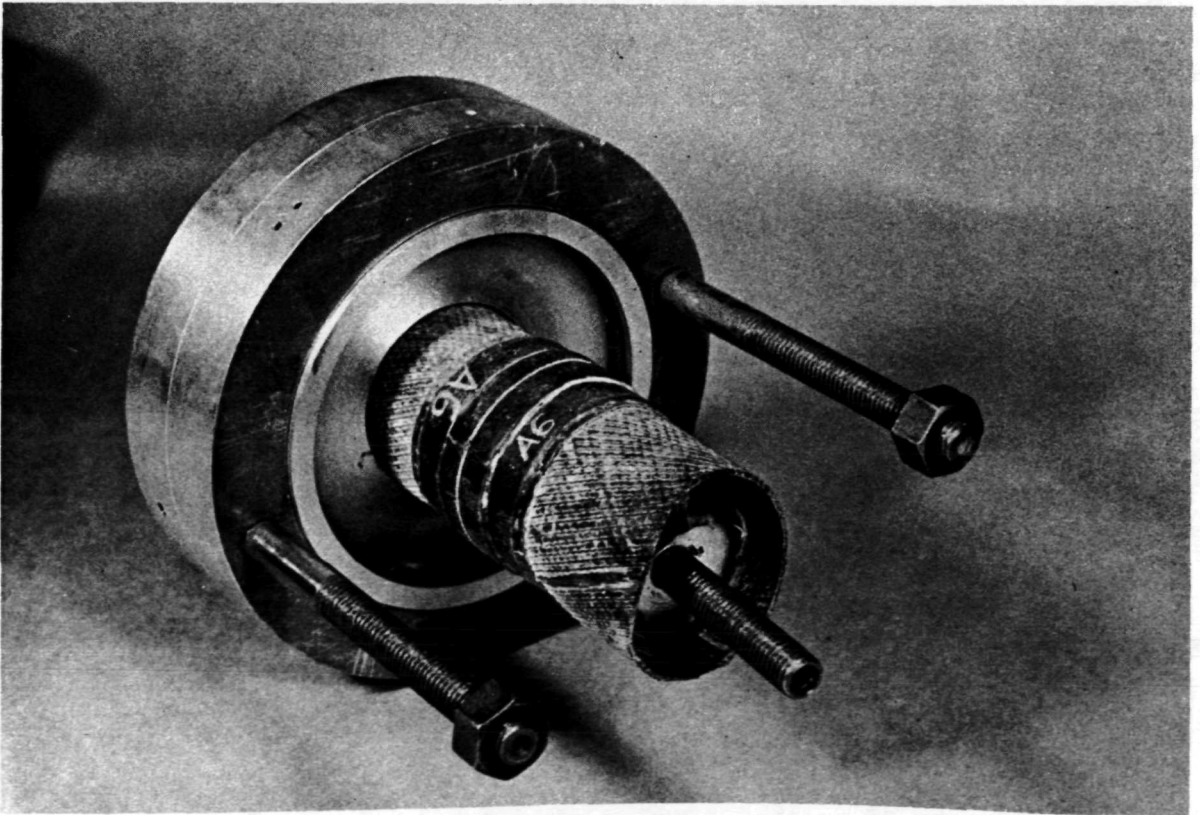
Figure 41. Bladder inserted in green tire.

Figure 42. Bladder and green tire inserted into one half the mold.

found for this work were short lengths of bicycle inner tube, although other materials were occasionally used. In commercial tire production a bladder is especially molded for this purpose, and that would undoubtedly be the best solution for the model tire.

The uncured tire and bladder are carfully positioned in the mold halves as shown in Figures 42 and 43, where in the latter photograph the two halves are partially closed together.

The partially closed mold halves are placed in a laboratory oven and attached to an air line. The bladder is slowly inflated as the mold halves are brought together. When they are completely closed, the air pressure is raised to 60 to 100 psi and the oven temperature to 360°F. The mold temperature is monitored with a contact pyrometer, and the time-temperature curve of the mold is integrated in an approximate, step-wise fashion to obtain the proper total cure.

The cured tire is removed from the mold and finished by cutting off the vents and end caps formed by the tapered plugs. Figure 44 shows tire A-6 after curing. The tire is then mounted on the rim, Figure 45, and exercised on the road wheel for three to four hours. The tire is now ready for mechanical property tests.
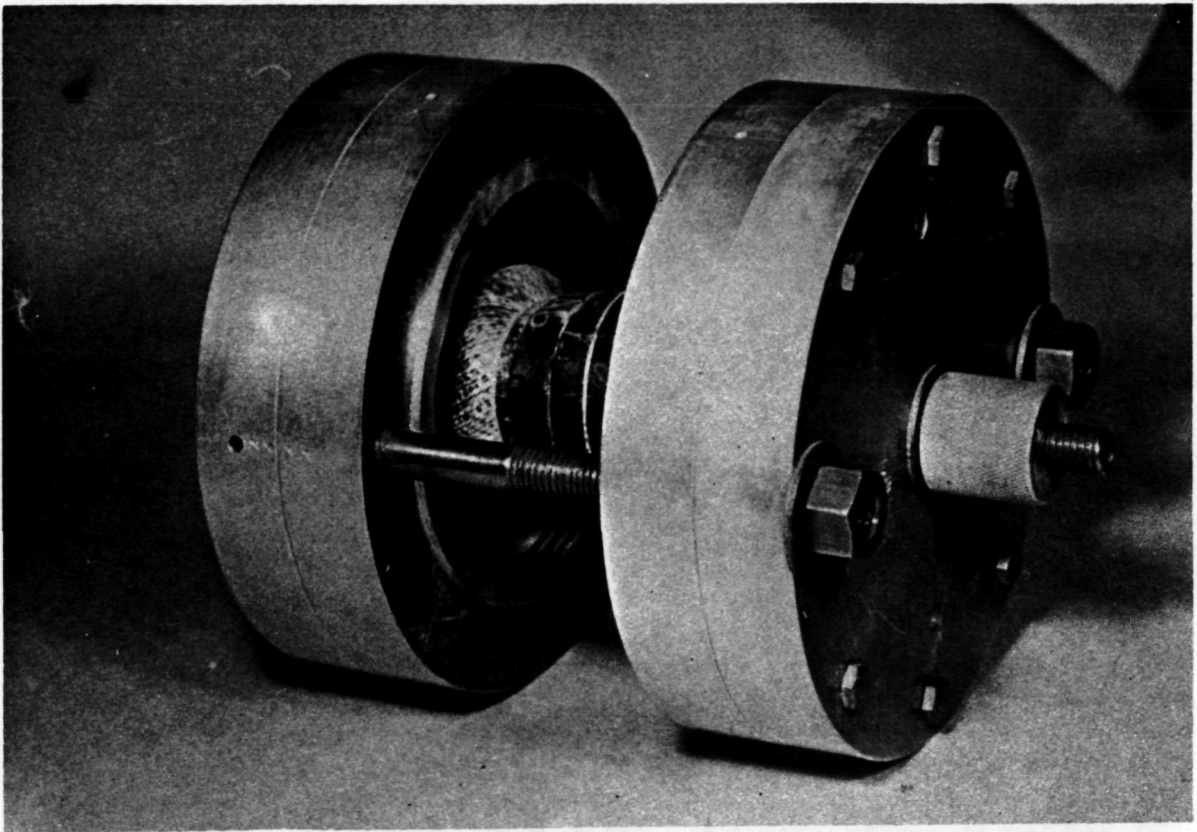
Figure 43. Mold assembly with green tire just visible, prior to lifting.
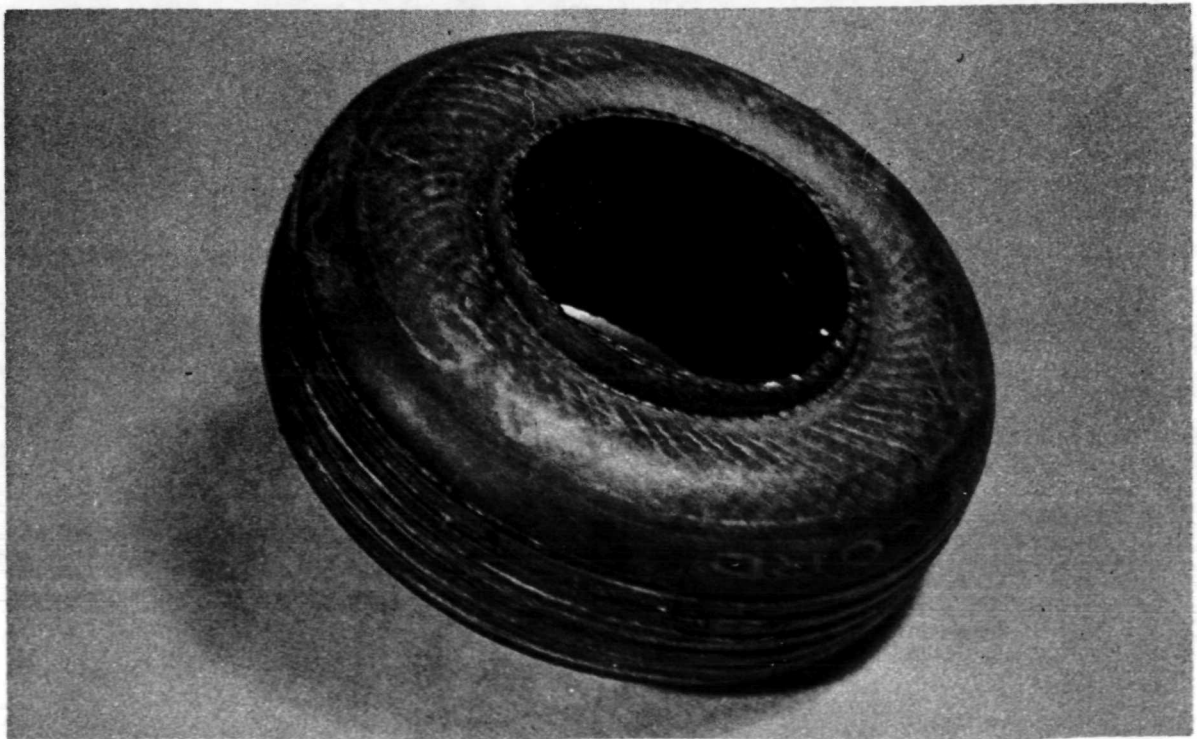

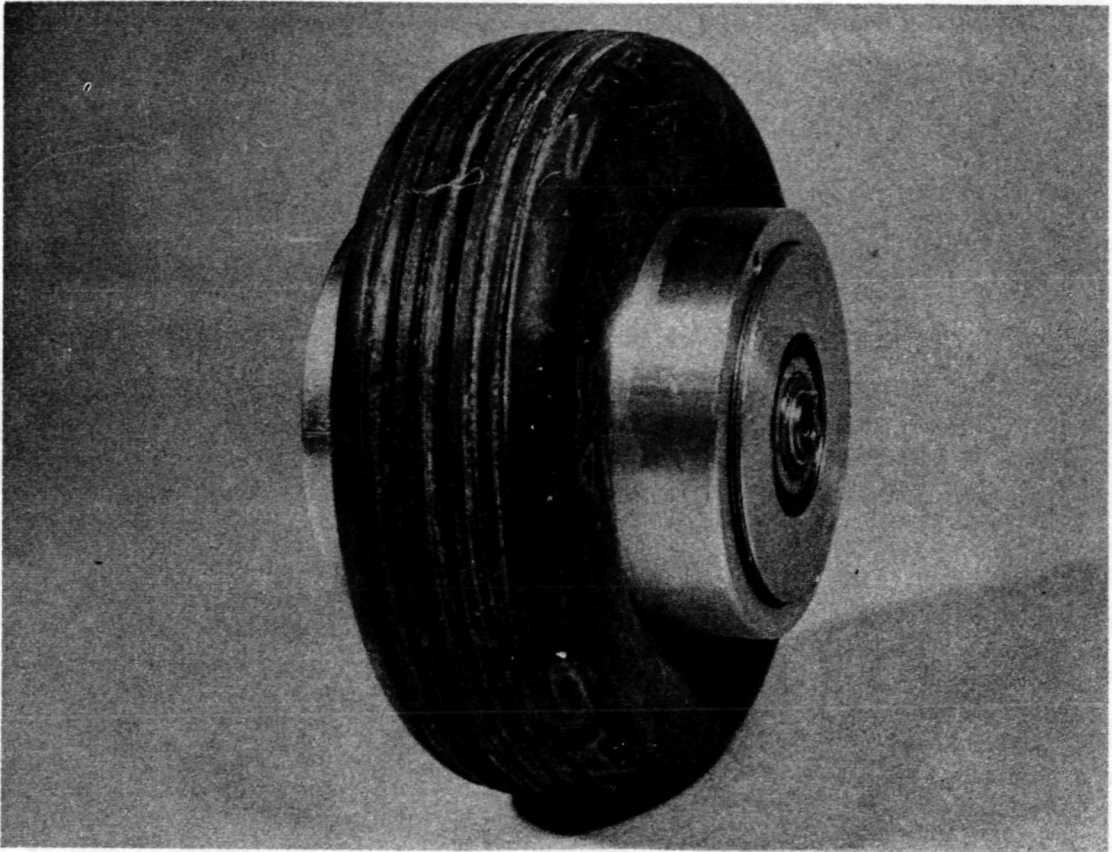Figure 44. Completed tire A-6 after removal from mold and trimming.

Figure 45.   Tire A-6 mounted on rim.

TIRE DEVELOPMENT

A number of tires were built and tested in order to develop the techniques described in this report. A complete description of this work would be prohibitively long. However, several important conclusions can be gleaned from the mass of accumulated experience. These are given below:

A.   The most important single property which the model tire builder must control is modulus of elasticity of the tire carcass, since this controls inflation pressures, loads and model test speeds.

B.   Tire carcass elasticity can be controlled by:

1.   End count of the fabric
2.   Number of plies used

68

3. Cord denier or modulus
4. Rubber modulus
5. Ply decoupling by means of a separator
6. Cord angle

All of these factors have been interplayed in the present work to produce a low modulus model tire, yet one whose modulus distribution is similar to that of the full size prototype.

C. Design changes can be readily seen in the model tires. For example, Table III describes a set of eight model tires, one purchased commercially and the other seven built especially for this project. Wide variations in structure are present, from conventional bias-ply to radial to pure rubber tires. Their dimensions are not too different from one another, yet their mechanical properties differ widely, as shown in Figure 46.

In general, it appears that the influence of tire structure should be as readily apparent in these model tires as in their full sized counterparts.

TABLE III

CONSTRUCTION AND DIMENSIONS OF TYPICAL "A" SERIES MODEL TIRES

| Type	A2 Bias	A3 Bias	A6 Bias	A7 Bias	A12 Radial	A17 Bias	VECO Rubber	A14 Bias
Cord-nylon	840/2	840/2	840/1	840/1	840/1	840/1 helical	-	840/2
Cut Green Angle	62°	62°	62°	62°	90°	57°	-	60°
Approximately Cured Crown Angle	40°	35°	40°	40°	90°	35°	-	35°
Approximate Rated Pressure, psi (using fore-aft method)	73	24	35	25	10	18	7	18
Tread	No	No	Yes	Yes	Yes	Yes	Yes	Yes
Dimensions (12.5 psi) Diameter	4.52	4.54	4.59	4.63	4.83	4.60	4.73	4.56
Width	1.56	1.62	1.61	1.68	1.49	1.72	1.82	1.61
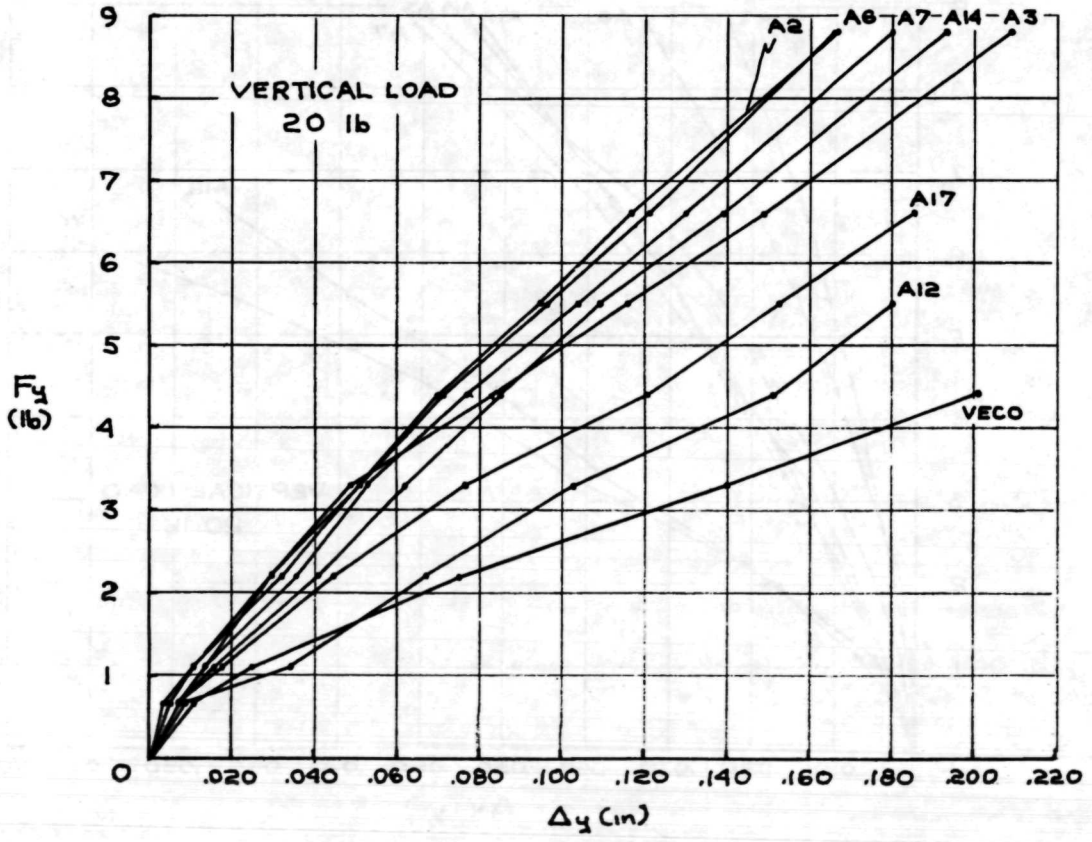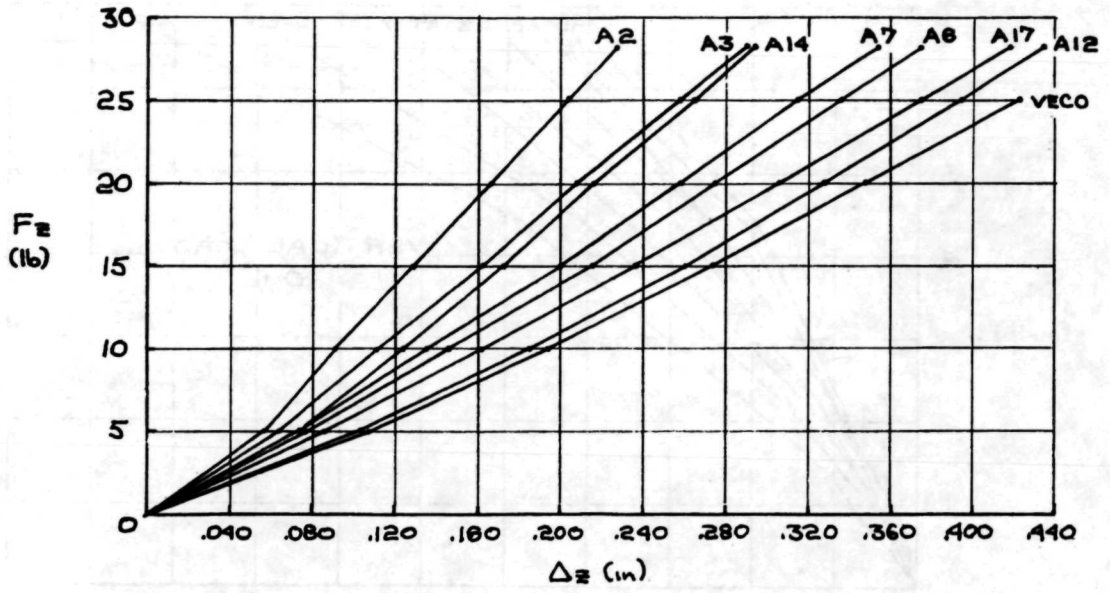
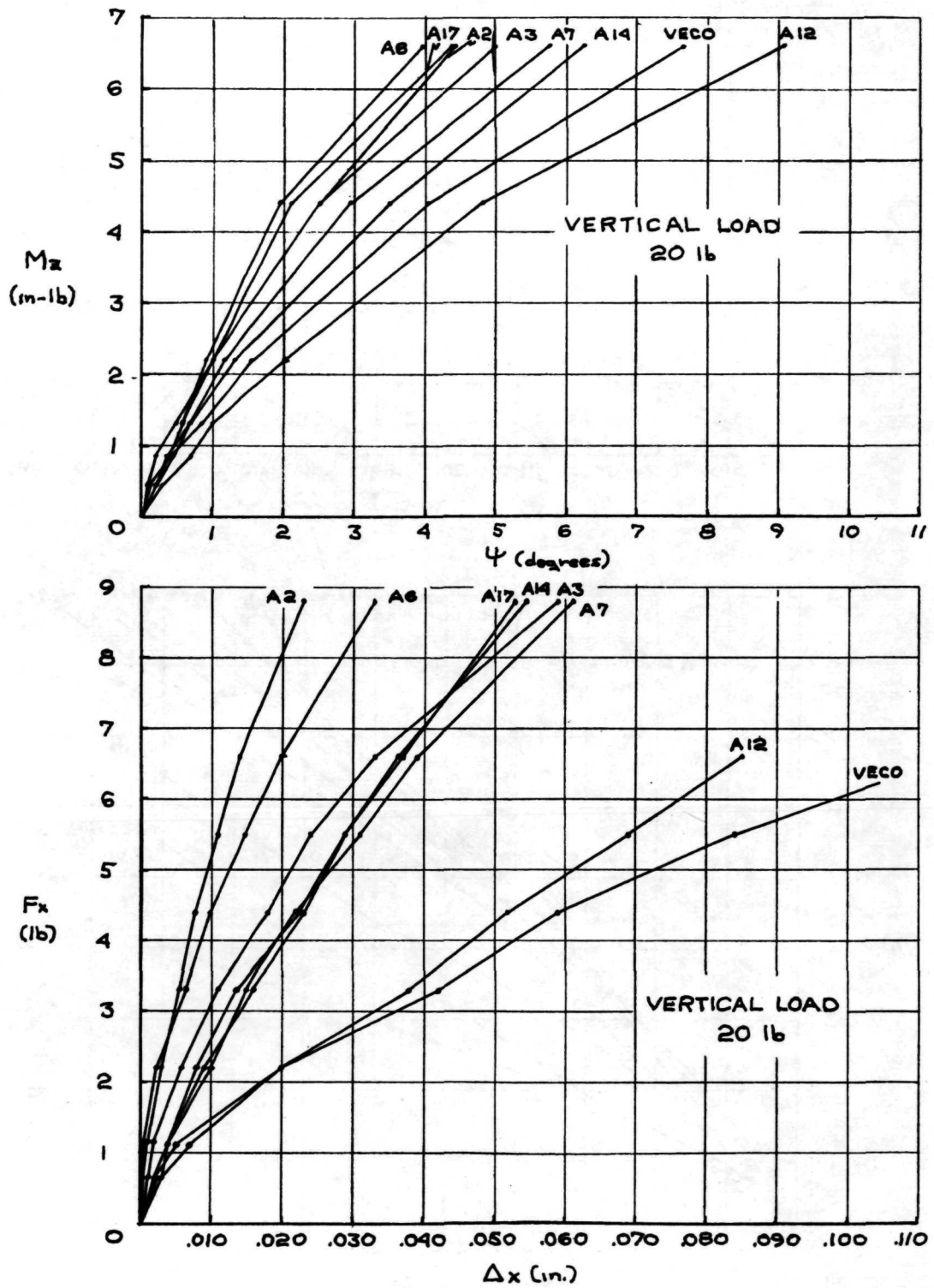Figure 46. Comparison of model tires static load-deflection at 12.5 psi inflation.

Figure 46. Concluded.

REFERENCES

[1] Langhaar, H. L., "Dimensional Analysis and Theory of Models," John Wiley and Sons, New York, 1951.

[2] Gordon, R. K., "Modeling of Tires," Soviet Rubber Technology, v. 24, n. 6, p. 30, 1965.

[3] Nybakken, G. H. and S. K. Clark, "Vertical and Lateral Stiffness Characteristics of Aircraft Tires," NASA CR-1488, National Aeronautics and Space Administration, Washington, D.C., 1969.

[4] Dodge, R. M., S. K. Clark, and K. L. Johnson, "An Analytical Model for Lateral Stiffness of Pneumatic Tires," The University of Michigan, Office of Research Administration, Report 02957-30-T, February 1967, Ann Arbor, Michigan.

[5] Dodge, R. N., D. Orne, and S. K. Clark, "Fore-and-Aft Stiffness Characteristics of Pneumatic Tires," NASA CR-900, National Aeronautics and Space Administration, Washington, D.C., October 1967.

[6] Horne, W. B., and R. F. Smiley, "Low Speed Yawed Rolling Characteristics and Other Elastic Properties of a Pair of 40 Inch Diameter 14 Ply Rating Type VII Aircraft Tires," N.A.C.A. Technical Note 4109, Washington, D.C., January 1958.

"The aeronautical and space activities of the United States shall be conducted so as to contribute . . . to the expansion of human knowledge of phenomena in the atmosphere and space. The Administration shall provide for the widest practicable and appropriate dissemination of information concerning its activities and the results thereof."
—NATIONAL AERONAUTICS AND SPACE ACT OF 1958

NASA SCIENTIFIC AND TECHNICAL PUBLICATIONS

TECHNICAL REPORTS: Scientific and technical information considered important, complete, and a lasting contribution to existing knowledge.

TECHNICAL NOTES: Information less broad in scope but nevertheless of importance as a contribution to existing knowledge.

TECHNICAL MEMORANDUMS: Information receiving limited distribution because of preliminary data, security classification, or other reasons. Also includes conference proceedings with either limited or unlimited distribution.

CONTRACTOR REPORTS: Scientific and technical information generated under a NASA contract or grant and considered an important contribution to existing knowledge.

TECHNICAL TRANSLATIONS: Information published in a foreign language considered to merit NASA distribution in English.

SPECIAL PUBLICATIONS: Information derived from or of value to NASA activities. Publications include final reports of major projects, monographs, data compilations, handbooks, sourcebooks, and special bibliographies.

TECHNOLOGY UTILIZATION PUBLICATIONS: Information on technology used by NASA that may be of particular interest in commercial and other non-aerospace applications. Publications include Tech Briefs, Technology Utilization Reports and Technology Surveys.

Details on the availability of these publications may be obtained from:

SCIENTIFIC AND TECHNICAL INFORMATION OFFICE

NATIONAL AERONAUTICS AND SPACE ADMINISTRATION
Washington, D.C. 20546